BABAR-PUB-12/015

SLAC-PUB-15208
arXiv:1208.1253 [hep-ex]

Branching fraction and form-factor shape measurements of exclusive charmless semileptonic B decays, and determination of $|V_{ub}|$

J. P. Lees, V. Poireau, and V. Tisserand
Laboratoire d'Annecy-le-Vieux de Physique des Particules (LAPP), Université de Savoie, CNRS/IN2P3, F-74941 Annecy-Le-Vieux, France

J. Garra Tico and E. Grauges
Universitat de Barcelona, Facultat de Fisica, Departament ECM, E-08028 Barcelona, Spain

A. Palano[ab]
INFN Sezione di Bari[a]; Dipartimento di Fisica, Università di Bari[b], I-70126 Bari, Italy

G. Eigen and B. Stugu
University of Bergen, Institute of Physics, N-5007 Bergen, Norway

D. N. Brown, L. T. Kerth, Yu. G. Kolomensky, and G. Lynch
Lawrence Berkeley National Laboratory and University of California, Berkeley, California 94720, USA

H. Koch and T. Schroeder
Ruhr Universität Bochum, Institut für Experimentalphysik 1, D-44780 Bochum, Germany

D. J. Asgeirsson, C. Hearty, T. S. Mattison, J. A. McKenna, and R. Y. So
University of British Columbia, Vancouver, British Columbia, Canada V6T 1Z1

A. Khan
Brunel University, Uxbridge, Middlesex UB8 3PH, United Kingdom

V. E. Blinov, A. R. Buzykaev, V. P. Druzhinin, V. B. Golubev, E. A. Kravchenko, A. P. Onuchin, S. I. Serednyakov, Yu. I. Skovpen, E. P. Solodov, K. Yu. Todyshev, and A. N. Yushkov
Budker Institute of Nuclear Physics, Novosibirsk 630090, Russia

M. Bondioli, D. Kirkby, A. J. Lankford, and M. Mandelkern
University of California at Irvine, Irvine, California 92697, USA

H. Atmacan, J. W. Gary, F. Liu, O. Long, and G. M. Vitug
University of California at Riverside, Riverside, California 92521, USA

C. Campagnari, T. M. Hong, D. Kovalskyi, J. D. Richman, and C. A. West
University of California at Santa Barbara, Santa Barbara, California 93106, USA

A. M. Eisner, J. Kroseberg, W. S. Lockman, A. J. Martinez, B. A. Schumm, and A. Seiden
University of California at Santa Cruz, Institute for Particle Physics, Santa Cruz, California 95064, USA

D. S. Chao, C. H. Cheng, B. Echenard, K. T. Flood, D. G. Hitlin, P. Ongmongkolkul, F. C. Porter, and A. Y. Rakitin
California Institute of Technology, Pasadena, California 91125, USA

R. Andreassen, Z. Huard, B. T. Meadows, M. D. Sokoloff, and L. Sun
University of Cincinnati, Cincinnati, Ohio 45221, USA

P. C. Bloom, W. T. Ford, A. Gaz, U. Nauenberg, J. G. Smith, and S. R. Wagner
University of Colorado, Boulder, Colorado 80309, USA

Work supported by US Department of Energy contract DE-AC02-76SF00515.

SLAC National Accelerator Laboratory, Menlo Park, CA 94025

R. Ayad* and W. H. Toki
Colorado State University, Fort Collins, Colorado 80523, USA

B. Spaan
Technische Universität Dortmund, Fakultät Physik, D-44221 Dortmund, Germany

K. R. Schubert and R. Schwierz
Technische Universität Dresden, Institut für Kern- und Teilchenphysik, D-01062 Dresden, Germany

D. Bernard and M. Verderi
Laboratoire Leprince-Ringuet, Ecole Polytechnique, CNRS/IN2P3, F-91128 Palaiseau, France

P. J. Clark and S. Playfer
University of Edinburgh, Edinburgh EH9 3JZ, United Kingdom

D. Bettoni[a], C. Bozzi[a], R. Calabrese[ab], G. Cibinetto[ab], E. Fioravanti[ab],
I. Garzia[ab], E. Luppi[ab], M. Munerato[ab], L. Piemontese[a], and V. Santoro[a]
INFN Sezione di Ferrara[a]; Dipartimento di Fisica, Università di Ferrara[b], I-44100 Ferrara, Italy

R. Baldini-Ferroli, A. Calcaterra, R. de Sangro, G. Finocchiaro,
P. Patteri, I. M. Peruzzi,† M. Piccolo, M. Rama, and A. Zallo
INFN Laboratori Nazionali di Frascati, I-00044 Frascati, Italy

R. Contri[ab], E. Guido[ab], M. Lo Vetere[ab], M. R. Monge[ab], S. Passaggio[a], C. Patrignani[ab], and E. Robutti[a]
INFN Sezione di Genova[a]; Dipartimento di Fisica, Università di Genova[b], I-16146 Genova, Italy

B. Bhuyan and V. Prasad
Indian Institute of Technology Guwahati, Guwahati, Assam, 781 039, India

C. L. Lee and M. Morii
Harvard University, Cambridge, Massachusetts 02138, USA

A. J. Edwards
Harvey Mudd College, Claremont, California 91711, USA

A. Adametz and U. Uwer
Universität Heidelberg, Physikalisches Institut, Philosophenweg 12, D-69120 Heidelberg, Germany

H. M. Lacker and T. Lueck
Humboldt-Universität zu Berlin, Institut für Physik, Newtonstr. 15, D-12489 Berlin, Germany

P. D. Dauncey
Imperial College London, London, SW7 2AZ, United Kingdom

U. Mallik
University of Iowa, Iowa City, Iowa 52242, USA

C. Chen, J. Cochran, W. T. Meyer, S. Prell, and A. E. Rubin
Iowa State University, Ames, Iowa 50011-3160, USA

A. V. Gritsan and Z. J. Guo
Johns Hopkins University, Baltimore, Maryland 21218, USA

N. Arnaud, M. Davier, D. Derkach, G. Grosdidier, F. Le Diberder, A. M. Lutz,
B. Malaescu, P. Roudeau, M. H. Schune, A. Stocchi, and G. Wormser
*Laboratoire de l'Accélérateur Linéaire, IN2P3/CNRS et Université Paris-Sud 11,
Centre Scientifique d'Orsay, B. P. 34, F-91898 Orsay Cedex, France*

D. J. Lange and D. M. Wright
Lawrence Livermore National Laboratory, Livermore, California 94550, USA

C. A. Chavez, J. P. Coleman, J. R. Fry, E. Gabathuler, D. E. Hutchcroft, D. J. Payne, and C. Touramanis
University of Liverpool, Liverpool L69 7ZE, United Kingdom

A. J. Bevan, F. Di Lodovico, R. Sacco, and M. Sigamani
Queen Mary, University of London, London, E1 4NS, United Kingdom

G. Cowan
University of London, Royal Holloway and Bedford New College, Egham, Surrey TW20 0EX, United Kingdom

D. N. Brown and C. L. Davis
University of Louisville, Louisville, Kentucky 40292, USA

A. G. Denig, M. Fritsch, W. Gradl, K. Griessinger, A. Hafner, and E. Prencipe
Johannes Gutenberg-Universität Mainz, Institut für Kernphysik, D-55099 Mainz, Germany

R. J. Barlow,[‡] G. Jackson, and G. D. Lafferty
University of Manchester, Manchester M13 9PL, United Kingdom

E. Behn, R. Cenci, B. Hamilton, A. Jawahery, and D. A. Roberts
University of Maryland, College Park, Maryland 20742, USA

C. Dallapiccola
University of Massachusetts, Amherst, Massachusetts 01003, USA

R. Cowan, D. Dujmic, and G. Sciolla
Massachusetts Institute of Technology, Laboratory for Nuclear Science, Cambridge, Massachusetts 02139, USA

R. Cheaib, D. Lindemann, P. M. Patel,[§] and S. H. Robertson
McGill University, Montréal, Québec, Canada H3A 2T8

P. Biassoni[ab], N. Neri[a], F. Palombo[ab], and S. Stracka[ab]
INFN Sezione di Milano[a]; Dipartimento di Fisica, Università di Milano[b], I-20133 Milano, Italy

L. Cremaldi, R. Godang,[¶] R. Kroeger, P. Sonnek, and D. J. Summers
University of Mississippi, University, Mississippi 38677, USA

X. Nguyen, M. Simard, and P. Taras
Université de Montréal, Physique des Particules, Montréal, Québec, Canada H3C 3J7

G. De Nardo[ab], D. Monorchio[ab], G. Onorato[ab], and C. Sciacca[ab]
INFN Sezione di Napoli[a]; Dipartimento di Scienze Fisiche,
Università di Napoli Federico II[b], I-80126 Napoli, Italy

M. Martinelli and G. Raven
NIKHEF, National Institute for Nuclear Physics and High Energy Physics, NL-1009 DB Amsterdam, The Netherlands

C. P. Jessop, J. M. LoSecco, and W. F. Wang
University of Notre Dame, Notre Dame, Indiana 46556, USA

K. Honscheid and R. Kass
Ohio State University, Columbus, Ohio 43210, USA

J. Brau, R. Frey, N. B. Sinev, D. Strom, and E. Torrence
University of Oregon, Eugene, Oregon 97403, USA

E. Feltresi[ab], N. Gagliardi[ab], M. Margoni[ab], M. Morandin[a],
M. Posocco[a], M. Rotondo[a], G. Simi[a], F. Simonetto[ab], and R. Stroili[ab]
INFN Sezione di Padova[a]; Dipartimento di Fisica, Università di Padova[b], I-35131 Padova, Italy

S. Akar, E. Ben-Haim, M. Bomben, G. R. Bonneaud, H. Briand, G. Calderini,
J. Chauveau, O. Hamon, Ph. Leruste, G. Marchiori, J. Ocariz, and S. Sitt
Laboratoire de Physique Nucléaire et de Hautes Energies,
IN2P3/CNRS, Université Pierre et Marie Curie-Paris6,
Université Denis Diderot-Paris7, F-75252 Paris, France

M. Biasini[ab], E. Manoni[ab], S. Pacetti[ab], and A. Rossi[ab]
INFN Sezione di Perugia[a]; Dipartimento di Fisica, Università di Perugia[b], I-06100 Perugia, Italy

C. Angelini[ab], G. Batignani[ab], S. Bettarini[ab], M. Carpinelli[ab],** G. Casarosa[ab], A. Cervelli[ab], F. Forti[ab],
M. A. Giorgi[ab], A. Lusiani[ac], B. Oberhof[ab], E. Paoloni[ab], A. Perez[a], G. Rizzo[ab], and J. J. Walsh[a]
INFN Sezione di Pisa[a]; Dipartimento di Fisica, Università di Pisa[b]; Scuola Normale Superiore di Pisa[c], I-56127 Pisa, Italy

D. Lopes Pegna, J. Olsen, A. J. S. Smith, and A. V. Telnov
Princeton University, Princeton, New Jersey 08544, USA

F. Anulli[a], R. Faccini[ab], F. Ferrarotto[a], F. Ferroni[ab], M. Gaspero[ab], L. Li Gioi[a], M. A. Mazzoni[a], and G. Piredda[a]
INFN Sezione di Roma[a]; Dipartimento di Fisica,
Università di Roma La Sapienza[b], I-00185 Roma, Italy

C. Bünger, O. Grünberg, T. Hartmann, T. Leddig, C. Voß, and R. Waldi
Universität Rostock, D-18051 Rostock, Germany

T. Adye, E. O. Olaiya, and F. F. Wilson
Rutherford Appleton Laboratory, Chilton, Didcot, Oxon, OX11 0QX, United Kingdom

S. Emery, G. Hamel de Monchenault, G. Vasseur, and Ch. Yèche
CEA, Irfu, SPP, Centre de Saclay, F-91191 Gif-sur-Yvette, France

D. Aston, D. J. Bard, R. Bartoldus, J. F. Benitez, C. Cartaro, M. R. Convery, J. Dorfan, G. P. Dubois-Felsmann,
W. Dunwoodie, M. Ebert, R. C. Field, M. Franco Sevilla, B. G. Fulsom, A. M. Gabareen, M. T. Graham,
P. Grenier, C. Hast, W. R. Innes, M. H. Kelsey, P. Kim, M. L. Kocian, D. W. G. S. Leith, P. Lewis, B. Lindquist,
S. Luitz, V. Luth, H. L. Lynch, D. B. MacFarlane, D. R. Muller, H. Neal, S. Nelson, M. Perl, T. Pulliam,
B. N. Ratcliff, A. Roodman, A. A. Salnikov, R. H. Schindler, A. Snyder, D. Su, M. K. Sullivan, J. Va'vra,
A. P. Wagner, W. J. Wisniewski, M. Wittgen, D. H. Wright, H. W. Wulsin, C. C. Young, and V. Ziegler
SLAC National Accelerator Laboratory, Stanford, California 94309 USA

W. Park, M. V. Purohit, R. M. White, and J. R. Wilson
University of South Carolina, Columbia, South Carolina 29208, USA

A. Randle-Conde and S. J. Sekula
Southern Methodist University, Dallas, Texas 75275, USA

M. Bellis, P. R. Burchat, T. S. Miyashita, and E. M. T. Puccio
Stanford University, Stanford, California 94305-4060, USA

M. S. Alam and J. A. Ernst
State University of New York, Albany, New York 12222, USA

R. Gorodeisky, N. Guttman, D. R. Peimer, and A. Soffer
Tel Aviv University, School of Physics and Astronomy, Tel Aviv, 69978, Israel

P. Lund and S. M. Spanier
University of Tennessee, Knoxville, Tennessee 37996, USA

J. L. Ritchie, A. M. Ruland, R. F. Schwitters, and B. C. Wray
University of Texas at Austin, Austin, Texas 78712, USA

J. M. Izen and X. C. Lou
University of Texas at Dallas, Richardson, Texas 75083, USA

F. Bianchi[ab], D. Gamba[ab], and S. Zambito[ab]
INFN Sezione di Torino[a]; Dipartimento di Fisica Sperimentale, Università di Torino[b], I-10125 Torino, Italy

L. Lanceri[ab] and L. Vitale[ab]
INFN Sezione di Trieste[a]; Dipartimento di Fisica, Università di Trieste[b], I-34127 Trieste, Italy

F. Martinez-Vidal, A. Oyanguren, and P. Villanueva-Perez
IFIC, Universitat de Valencia-CSIC, E-46071 Valencia, Spain

H. Ahmed, J. Albert, Sw. Banerjee, F. U. Bernlochner, H. H. F. Choi, G. J. King, R. Kowalewski, M. J. Lewczuk, I. M. Nugent, J. M. Roney, R. J. Sobie, and N. Tasneem
University of Victoria, Victoria, British Columbia, Canada V8W 3P6

T. J. Gershon, P. F. Harrison, and T. E. Latham
Department of Physics, University of Warwick, Coventry CV4 7AL, United Kingdom

H. R. Band, S. Dasu, Y. Pan, R. Prepost, and S. L. Wu
University of Wisconsin, Madison, Wisconsin 53706, USA

We report the results of a study of the exclusive charmless semileptonic decays, $B^0 \to \pi^-\ell^+\nu$, $B^+ \to \pi^0\ell^+\nu$, $B^+ \to \omega\ell^+\nu$, $B^+ \to \eta\ell^+\nu$ and $B^+ \to \eta'\ell^+\nu$, ($\ell = e$ or μ) undertaken with approximately 462×10^6 $B\bar{B}$ pairs collected at the $\Upsilon(4S)$ resonance with the *BABAR* detector. The analysis uses events in which the signal B decays are reconstructed with a loose neutrino reconstruction technique. We obtain partial branching fractions in several bins of q^2, the square of the momentum transferred to the lepton-neutrino pair, for $B^0 \to \pi^-\ell^+\nu$, $B^+ \to \pi^0\ell^+\nu$, $B^+ \to \omega\ell^+\nu$ and $B^+ \to \eta\ell^+\nu$. From these distributions, we extract the form-factor shapes $f_+(q^2)$ and the total branching fractions $\mathcal{B}(B^0 \to \pi^-\ell^+\nu) = (1.45 \pm 0.04_{stat} \pm 0.06_{syst}) \times 10^{-4}$ (combined π^- and π^0 decay channels assuming isospin symmetry), $\mathcal{B}(B^+ \to \omega\ell^+\nu) = (1.19 \pm 0.16_{stat} \pm 0.09_{syst}) \times 10^{-4}$ and $\mathcal{B}(B^+ \to \eta\ell^+\nu) = (0.38 \pm 0.05_{stat} \pm 0.05_{syst}) \times 10^{-4}$. We also measure $\mathcal{B}(B^+ \to \eta'\ell^+\nu) = (0.24 \pm 0.08_{stat} \pm 0.03_{syst}) \times 10^{-4}$. We obtain values for the magnitude of the CKM matrix element $|V_{ub}|$ by direct comparison with three different QCD calculations in restricted q^2 ranges of $B \to \pi\ell^+\nu$ decays. From a simultaneous fit to the experimental data over the full q^2 range and the FNAL/MILC lattice QCD predictions, we obtain $|V_{ub}| = (3.25 \pm 0.31) \times 10^{-3}$, where the error is the combined experimental and theoretical uncertainty.

PACS numbers: 13.20.He, 12.15.Hh, 12.38.Qk, 14.40.Nd

I. INTRODUCTION

A precise measurement of the CKM matrix [1] element $|V_{ub}|$ will improve our quantitative understanding of weak interactions and CP violation in the Standard Model. The value of $|V_{ub}|$ can be determined by the measurement of the partial branching fractions of exclusive charmless semileptonic B decays since the rate for decays that involve a scalar meson is proportional to $|V_{ub}f_+(q^2)|^2$. Here, the form factor $f_+(q^2)$ depends on q^2, the square of the momentum transferred to the lepton-neutrino pair. Values of $f_+(q^2)$ can be calculated at small q^2 ($\lesssim 16$ GeV^2) using Light Cone Sum Rules (LCSR) [2–4] and at large q^2 ($\gtrsim 16$ GeV^2) from unquenched Lattice QCD (LQCD) [5, 6]. Extraction of the $f_+(q^2)$ form-factor shapes from exclusive decays [7] such as $B^0 \to \pi^-\ell^+\nu$ [8–10], $B^+ \to \pi^0\ell^+\nu$ [8], $B^+ \to \omega\ell^+\nu$ [11] and $B^+ \to \eta^{(\prime)}\ell^+\nu$ [9] may be used to test these theoretical predictions [12]. Measurements of the branching fractions (BF) of all these decays will also improve our knowledge of the composition of charmless

*Now at the University of Tabuk, Tabuk 71491, Saudi Arabia
†Also with Università di Perugia, Dipartimento di Fisica, Perugia, Italy
‡Now at the University of Huddersfield, Huddersfield HD1 3DH, UK
§Deceased
¶Now at University of South Alabama, Mobile, Alabama 36688, USA
**Also with Università di Sassari, Sassari, Italy

semileptonic decays. This input can be used to reduce the large systematic uncertainty in $|V_{ub}|$ due to the poorly known $b \to u\ell\nu$ signal composition in inclusive semileptonic B decays. It will also help to constrain the size of the gluonic singlet contribution to form factors for the $B^+ \to \eta^{(\prime)}\ell^+\nu$ decays [4, 13].

In this paper, we present measurements of the partial BFs $\Delta\mathcal{B}(B^0 \to \pi^-\ell^+\nu, q^2)$ in 12 bins of q^2, $\Delta\mathcal{B}(B^+ \to \pi^0\ell^+\nu, q^2)$ in 11 bins of q^2, $\Delta\mathcal{B}(B^+ \to \omega\ell^+\nu, q^2)$ and $\Delta\mathcal{B}(B^+ \to \eta\ell^+\nu, q^2)$ in five bins of q^2, as well as the BF $\mathcal{B}(B^+ \to \eta'\ell^+\nu)$. From these distributions, we extract the total BFs for each of the five decay modes. Values of these BFs were previously reported in Refs. [8–11], and references therein. In this work, we carry out an untagged analysis (*i.e.* the second B meson is not explicitly reconstructed) with the loose neutrino reconstruction technique [14] whereby the selections on the variables required to reconstruct the neutrino are much looser than usual. This results in a large candidate sample. Concerning the $B^+ \to \pi^0\ell^+\nu$ and $B^+ \to \omega\ell^+\nu$ decay modes, this is the first analysis using this technique.

We assume isospin symmetry to hold, and combine the data of the $B^+ \to \pi^0\ell^+\nu$ and $B^0 \to \pi^-\ell^+\nu$ channels thereby leading to a large increase, of the order of 34%, in the effective number of $B^0 \to \pi^-\ell^+\nu$ events available for study. We refer to such events as $B \to \pi\ell^+\nu$ decays. The values of the BFs obtained in the present work are based on the use of the most recent BFs and form-factor shapes for all decay channels in our study. In particular, the subsequent improved treatment of the distributions that describe the combination of resonant and nonresonant $b \to u\ell\nu$ decays results in an increase of 3.5% in the total BF value of the $B^0 \to \pi^-\ell^+\nu$ decays. This increase is significant in view of the total uncertainty of 5.1% obtained in the measurement of this BF.

We now optimize our selections over the entire fit region instead of the signal-enhanced region, as was done previously [9]. The ensuing tighter selections produce a data set with a better signal to background ratio and higher purity in the $B^0 \to \pi^-\ell^+\nu$ and $B^+ \to \eta^{(\prime)}\ell^+\nu$ decays. As a result, we can now investigate the $B^+ \to \eta^{(\prime)}\ell^+\nu$ decays over their full q^2 ranges. The present analysis of the $B^0 \to \pi^-\ell^+\nu$ decay channel makes use of the full *BABAR* data set compared to only a subset in Ref. [8]. As for the $B^+ \to \omega\ell^+\nu$ decay channel, it uses the unfolded values of the partial BFs and a selection procedure that is significantly different from the one in Ref. [11]. The unfolding process is used to obtain the distribution of the true values of q^2 by applying the inverse of the detector response matrix to the distribution of the measured values of q^2. Each element of this matrix is constructed in MC simulation for each bin of q^2 as the ratio of the number of true events to the total number of reconstructed events. The current work provides results for five decay channels using the same analysis method.

In this work, we compare the values of $\Delta\mathcal{B}(q^2)$ for the $B \to \pi\ell^+\nu$ mode to form-factor calculations [2, 3, 5, 6] in restricted q^2 ranges to obtain values of $|V_{ub}|$. Values of $|V_{ub}|$ with a smaller total uncertainty can also be obtained from a simultaneous fit to the $B \to \pi\ell^+\nu$ experimental data over the full q^2 range and the FNAL/MILC lattice QCD predictions [6]. Such values were recently obtained by *BABAR* [8] ($|V_{ub}| = (2.95 \pm 0.31) \times 10^{-3}$) and Belle [10] ($|V_{ub}| = (3.43 \pm 0.33) \times 10^{-3}$). These results are consistent at the 2σ level, when taking into account the correlations, but display a tension with respect to the value of $|V_{ub}|$ measured [12] in inclusive semileptonic B decays, $|V_{ub}| = (4.27 \pm 0.38) \times 10^{-3}$. This study attempts to resolve the tension by analyzing the data using the most recent values of BFs and form factors.

II. DATA SAMPLE AND SIMULATION

We use a sample of 462×10^6 $B\bar{B}$ pairs, corresponding to an integrated luminosity of 416.1 fb^{-1}, collected at the $\Upsilon(4S)$ resonance with the *BABAR* detector [15] at the PEP-II asymmetric-energy e^+e^- storage rings. A sample of 43.9 fb^{-1} collected approximately 40 MeV below the $\Upsilon(4S)$ resonance (denoted "off-resonance data") is used to study contributions from $e^+e^- \to u\bar{u}/d\bar{d}/s\bar{s}/c\bar{c}/\tau^+\tau^-$ (continuum) events. Detailed Monte Carlo (MC) simulations are used to optimize the signal selections, estimate the signal efficiencies, obtain the shapes of the signal and background distributions and determine the systematic uncertainties associated with the BF values.

MC samples are generated for $\Upsilon(4S) \to B\bar{B}$ events, continuum events, and dedicated signal samples containing $B^0 \to \pi^-\ell^+\nu$, $B^+ \to \pi^0\ell^+\nu$, $B^+ \to \omega\ell^+\nu$ and $B^+ \to \eta^{(\prime)}\ell^+\nu$ signal decays, separately. These signal MC events are produced with the FLATQ2 generator [16]. The $f_+(q^2)$ shape used in this generator is adjusted by reweighting the generated events. For the $B \to \pi\ell^+\nu$ decays, the signal MC events are reweighted to reproduce the Boyd-Grinstein-Lebed (BGL) parametrization [17], where the parameters are taken from Ref. [9]. For the $B^+ \to \omega\ell^+\nu$ decays, the events are reweighted to reproduce the Ball parametrization [18]. For the $B^+ \to \eta^{(\prime)}\ell^+\nu$ decays, the signal MC events are reweighted to reproduce the Becirevic-Kaidalov (BK) parametrization [19], where the parameter $\alpha_{BK} = 0.52 \pm 0.04$ gave a reasonable fit to the $B^0 \to \pi^-\ell^+\nu$ and $B^+ \to \eta\ell^+\nu$ data of Ref. [9]. The *BABAR* detector's acceptance and response are simulated using the GEANT4 package [20].

III. EVENT RECONSTRUCTION AND CANDIDATE SELECTION

To reconstruct the decays $B^0 \to \pi^-\ell^+\nu$, $B^+ \to \pi^0\ell^+\nu$, $B^+ \to \omega\ell^+\nu$ and $B^+ \to \eta^{(\prime)}\ell^+\nu$, we first reconstruct the final state meson. The ω meson is reconstructed in the $\omega \to \pi^+\pi^-\pi^0$ decay channel. The η meson is reconstructed in the $\eta \to \gamma\gamma$ ($\eta(\gamma\gamma)$) and $\eta \to \pi^+\pi^-\pi^0$ ($\eta(3\pi)$) decay channels while the η' is reconstructed in the $\eta' \to \eta\pi^+\pi^-$ decay channel, followed by the $\eta \to \gamma\gamma$

decay ($\eta'(\gamma\gamma)$). The $\eta' \to \rho^0\gamma$ decay channel suffers from large backgrounds and we do not consider it in the present work.

Event reconstruction with the *BABAR* detector is described in detail elsewhere [15]. Electrons and muons are mainly identified by their characteristic signatures in the electromagnetic calorimeter and the muon detector, respectively, while charged hadrons are identified and reconstructed using the silicon vertex tracker, the drift chamber and the Cherenkov detector. The photon and charged particle tracking reconstruction efficiencies are corrected using various control samples. The average electron and muon reconstruction efficiencies are 93% and 70%, respectively, while the corresponding probabilities that a pion is identified as a lepton are less than 0.2% and less than 1.5%, respectively.

The neutrino four-momentum, $P_\nu = (|\vec{p}^{\,*}_{miss}|, \vec{p}^{\,*}_{miss})$, is inferred from the difference between the momentum of the colliding-beam particles $\vec{p}^{\,*}_{beams}$ and the vector sum of the momenta of all the particles detected in the event $\vec{p}^{\,*}_{tot}$, such that $\vec{p}^{\,*}_{miss} = \vec{p}^{\,*}_{beams} - \vec{p}^{\,*}_{tot}$. All variables with an asterisk are given in the $\Upsilon(4S)$ frame. To evaluate E_{tot}, the total energy of all detected particles, we assume zero mass for all neutral candidates, and we use the known masses for the charged particles identified in the event. If the particle is not identified, its mass is assumed to be that of a pion.

In this analysis, we calculate the momentum transfer squared as $q^2 = (P_B - P_{meson})^2$ instead of $q^2 = (P_\ell + P_\nu)^2$, where P_B, P_{meson} and P_ℓ are the four-momenta of the B meson, of the π, ω, η or η' meson, and of the lepton, respectively, evaluated in the $\Upsilon(4S)$ frame. With this choice, the value of q^2 is unaffected by any misreconstruction of the neutrino. To maintain this advantage, P_B must be evaluated without any reference to the neutrino. It has an effective value since the magnitude of the 3-momentum $\vec{p}^{\,*}_B$ is determined from the center-of-mass energy and the known B meson mass but the direction of the B meson cannot be measured. It can only be estimated.

To do this, we first combine the lepton with a π, ω, η or η' meson to form the so-called Y pseudoparticle such that $P_Y = P_\ell + P_{meson}$. The angle θ_{BY}, between the Y and B momenta in the $\Upsilon(4S)$ frame, can be determined under the assumption that the only unobserved decay product is a neutrino, *i.e.*, $B \to Y\nu$. In this frame, the Y momentum, the B momentum and the angle θ_{BY} define a cone with the Y momentum as its axis and with a true B momentum lying somewhere on the surface of the cone. The B rest frame is thus known up to an azimuthal angle ψ about the Y momentum. The value of q^2 is then computed, as explained in Ref. [21], as the average of four q^2 values corresponding to four possible angles, ψ, $\psi+\pi/2$, $\psi+\pi$, $\psi+3\pi/2$ rad, where the angle ψ is chosen randomly. The four values of q^2 are weighted by the factor $\sin^2\theta_B$, θ_B being the angle between the B direction and the beam direction in the $\Upsilon(4S)$ frame. This weight is needed since $B\bar{B}$ production follows a $\sin^2\theta_B$ distribution in the $\Upsilon(4S)$ frame. We require that $|\cos\theta_{BY}| \leq 1$. We correct for the reconstruction effects on the measured values of q^2 (the q^2 resolution is approximately 0.6 GeV^2) by applying an unregularized unfolding algorithm to the measured q^2 spectra [22].

The selections of the candidate events are determined in MC simulation by maximizing the ratio $S/\sqrt{(S+B)}$ over the entire fit region, where S is the number of correctly reconstructed signal events and B is the total number of background events. The continuum background is suppressed by requiring the ratio of second to zeroth Fox-Wolfram moments [23] to be smaller than 0.5. Radiative Bhabha and two-photon processes are rejected by requirements on the number of charged particle tracks and neutral calorimeter clusters [24]. To ensure all track momenta are well measured, their polar angles are required to lie between 0.41 and 2.46 rad with respect to the electron beam direction (the acceptance of the detector). For all decays, we demand the momenta of the lepton and meson candidates to be topologically compatible with a real signal decay by requiring that a mass-constrained geometrical vertex fit [25] of the tracks associated with the two particles gives a χ^2 probability greater than 1%. In the fit, the external constraints such as reconstructed tracks are treated first, followed by all four-momenta conservation constraints. Finally, at each vertex, the geometric constraints and the mass are combined. These combined constraints are applied consecutively.

To reduce the number of unwanted leptons and secondary decays such as $D \to X\ell\nu$, J/ψ, τ and kaon decays, the minimum transverse momentum is 50 MeV for all leptons and 30 MeV for all photons, and all electron (muon) tracks are required to have momenta greater than 0.5 (1.0) GeV in the laboratory frame. The momenta of the lepton and the meson are further restricted to enhance signal over background. We require the following:

- for $B \to \pi\ell^+\nu$ decays:
  $|\vec{p}^{\,*}_\ell| > 2.2$ GeV or $|\vec{p}^{\,*}_\pi| > 1.3$ GeV
  or $|\vec{p}^{\,*}_\ell| + |\vec{p}^{\,*}_\pi| > 2.8$ GeV;
- for $B^+ \to \omega\ell^+\nu$ decays:
  $|\vec{p}^{\,*}_\ell| > 2.0$ GeV or $|\vec{p}^{\,*}_\omega| > 1.3$ GeV
  or $|\vec{p}^{\,*}_\ell| + |\vec{p}^{\,*}_\omega| > 2.65$ GeV;
- for $B^+ \to \eta\ell^+\nu$ decays:
  $|\vec{p}^{\,*}_\ell| > 2.1$ GeV or $|\vec{p}^{\,*}_\eta| > 1.3$ GeV
  or $|\vec{p}^{\,*}_\ell| + |\vec{p}^{\,*}_\eta| > 2.8$ GeV;
- for $B^+ \to \eta'\ell^+\nu$ decays:
  $|\vec{p}^{\,*}_\ell| > 2.0$ GeV or $|\vec{p}^{\,*}_{\eta'}| > 1.65$ GeV
  or $0.69|\vec{p}^{\,*}_\ell| + |\vec{p}^{\,*}_{\eta'}| > 2.4$ GeV.

These cuts primarily reject background and reduce the signal efficiencies by less than 5%.

To remove $J/\psi \to \mu^+\mu^-$ decays, we reject any combination of two muons, including misidentified pions, if the two particles have an invariant mass consistent with the J/ψ mass [3.07-3.13] GeV. We do not apply a specific J/ψ veto for $J/\psi \to e^+e^-$ decays, since we find no

evidence for any remaining such events in our data set. We restrict the reconstructed masses of the meson to lie in the interval:

- for $B^+ \to \pi^0\ell^+\nu$ decays: $0.115 < m_{\pi^0} < 0.150$ GeV,
- for $B^+ \to \omega\ell^+\nu$ decays: $0.760 < m_\omega < 0.805$ GeV,
- for $B^+ \to \eta\ell^+\nu$ decays: $0.51 < m_\eta < 0.57$ GeV,
- for $B^+ \to \eta'\ell^+\nu$ decays: $0.92 < m_{\eta'} < 0.98$ GeV.

Backgrounds are further reduced by q^2-dependent selections on the cosine of the angle, $\cos\theta_{thrust}$, between the thrust axes [26] of the Y and of the rest of the event; on the polar angle, θ_{miss}, associated with $\vec{p}_{miss}$; on the invariant missing mass squared, $m^2_{miss} = E^2_{miss} - |\vec{p}_{miss}|^2$, divided by twice the missing energy ($E_{miss} = E_{beams} - E_{tot}$); on the cosine of the angle, $\cos\theta_\ell$, between the direction of the virtual W boson (ℓ and ν combined) boosted in the rest frame of the B meson and the direction of the lepton boosted in the rest frame of the W boson; and on L2, the momentum weighted Legendre monomial of order 2. The quantity $m^2_{miss}/2E_{miss}$ should be consistent with zero if a single neutrino is missing. The phrase "rest of the event" refers to all the particles left in the event after the lepton and the meson used to form the Y pseudoparticle are removed.

The q^2-dependent selections are shown in the panels on the left-hand side of Fig. 1, and their effects are illustrated in the panels on the right-hand side of the same figure, for $B^0 \to \pi^-\ell^+\nu$ decays. A single vertical line indicates a fixed cut, a set of two vertical lines represents a q^2-dependent cut. The position of the two lines corresponds to the minimum and maximum values of the selection, shown in the left-hand side panels. The functions describing the q^2 dependence are given in Tables VIII-XIII of the Appendix for the five decays under study. For $B^+ \to \eta\ell^+\nu$ decays, additional background is rejected by requiring that $|\cos\theta_V| < 0.95$, where θ_V is the helicity angle of the η meson [16].

The kinematic variables $\Delta E = (P_B \cdot P_{beams} - s/2)/\sqrt{s}$ and $m_{ES} = \sqrt{(s/2 + \vec{p}_B \cdot \vec{p}_{beams})^2/E^2_{beams} - \vec{p}^2_B}$ are used in a fit to provide discrimination between signal and background decays. $\sqrt{s}$ is the center-of-mass energy of the colliding particles. Here, $P_B = P_{meson} + P_\ell + P_\nu$ must be evaluated in the laboratory frame. We only retain candidates with $|\Delta E| < 1.0$ GeV and $m_{ES} > 5.19$ GeV, thereby removing from the fit a region with large backgrounds. Fewer than 6.6% (12.5%, 7.2%, 7.4%, 1.9%) of all $\pi^-\ell\nu$ ($\pi^0\ell\nu$, $\omega\ell\nu$, $\eta\ell\nu$, $\eta'\ell\nu$) events have more than one candidate per event. For events with multiple candidates, only the candidate with the largest value of $\cos\theta_\ell$ is kept. The signal event reconstruction efficiency varies between 6.1% and 8.5% for $B^0 \to \pi^-\ell^+\nu$ decays, between 2.8% and 6.0% for $B^+ \to \pi^0\ell^+\nu$ decays, between 1.0% and 2.2% for $B^+ \to \omega\ell^+\nu$ decays, and between 0.9% and 2.6% for $B^+ \to \eta\ell^+\nu$ decays ($\gamma\gamma$ channel), depending on the value of q^2. The efficiency is 0.6% for

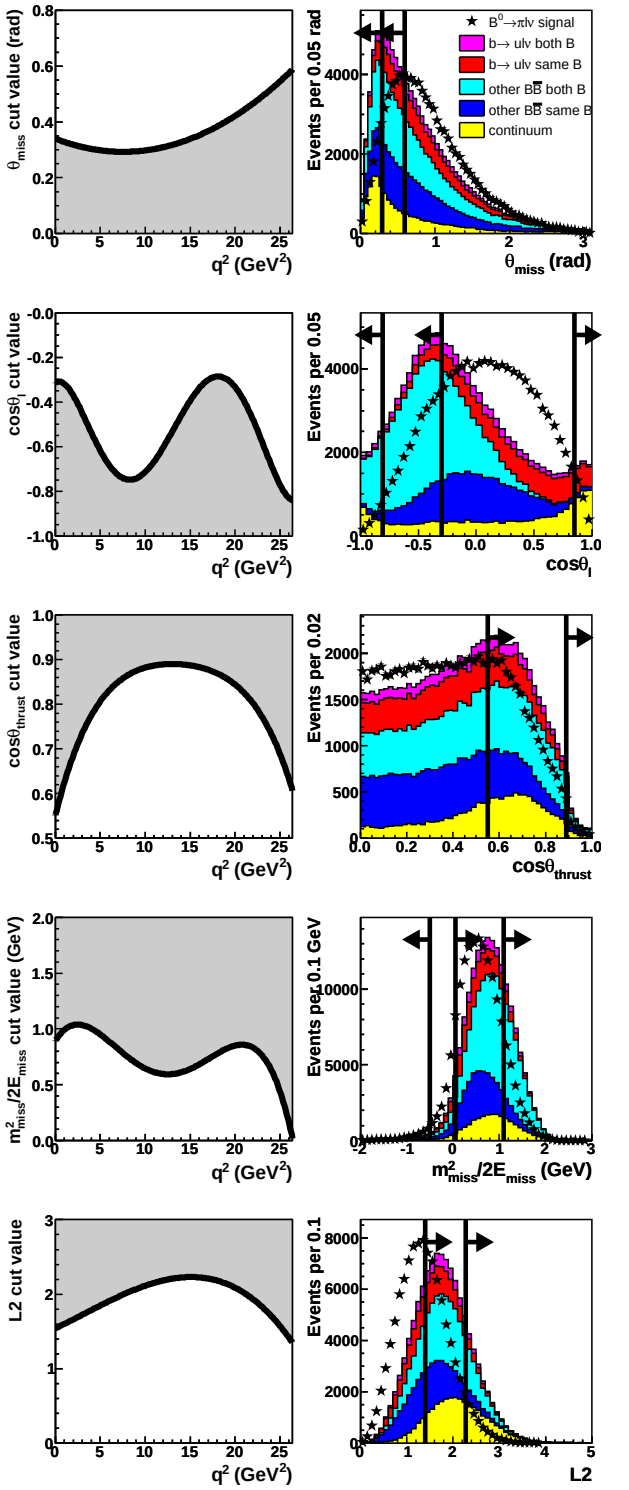

FIG. 1: (color online) Left panels: Distributions of the selection values for the q^2-dependent selections on the variables used in the analysis of $B^0 \to \pi^-\ell^+\nu$ decays. The vertical axis represents the selection value for a given q^2 value. We reject an event when its value is in the shaded region. Right panels: Corresponding distributions in the total fit region illustrating the effects of the q^2-dependent selections. The arrows indicate the rejected regions, as explained in the text. All the selections have been applied except for the one of interest. In each panel, the signal area is scaled to the area of the total background.

both $B^+ \to \eta\ell^+\nu$ ($\pi^+\pi^-\pi^0$ channel) and $B^+ \to \eta'\ell^+\nu$ decays. The efficiencies are given as a function of q^2 in Tables XXIII-XXVII of the Appendix.

IV. BACKGROUNDS AND SIGNAL EXTRACTION

Backgrounds can be broadly grouped into three main categories: decays arising from $b \to u\ell\nu$ transitions (other than the signal), decays in other $B\bar{B}$ events (excluding $b \to u\ell\nu$) and decays in continuum events. The "other $B\bar{B}$" background is the sum of different contributions, where more than 75% are from $B \to D/D^*/D^{**}$ decays. For the $B^0 \to \pi^-\ell^+\nu$, $B^+ \to \pi^0\ell^+\nu$ and combined $B \to \pi\ell^+\nu$ modes, for which there is a large number of candidate events, each of the first two categories of background is further split into a background category where the pion and the lepton come from the decay of the same B meson ("same-B" category), and a background category where the pion and the lepton come from the decay of different B mesons ("both-B" category).

We use the ΔE-m_{ES} histograms, obtained from the MC simulation, as two-dimensional probability density functions (PDFs) in an extended binned maximum-likelihood fit [27] to the data to extract the yields of the signal and backgrounds as a function of q^2. This fit method incorporates the statistical uncertainty from the finite MC sample size into the fit uncertainty. The ΔE-m_{ES} plane is subdivided into 34 bins for each bin of q^2 in the fits to the $\pi^-\ell^+\nu$, $\pi^0\ell^+\nu$ and $\pi\ell^+\nu$ candidate data where we have a reasonably large number of events, and into 19 bins in the fits to the $\omega\ell^+\nu$, $\eta\ell^+\nu$ and $\eta'\ell\nu$ decay data. The ΔE-m_{ES} distributions for the $B^0 \to \pi^-\ell^+\nu$ decay channel are shown in Fig. 2. The binning used in this case is also displayed in the figure. We use variable bin sizes because we want to have a large number of small bin sizes in the signal-enhanced region to better define this specific region. The signal-enhanced region is the region of the ΔE-m_{ES} plane with a large proportion of signal events. It is delimited in our work by the boundaries: $-0.16 < \Delta E < 0.20$ GeV and $m_{ES} > 5.268$ GeV (see Fig. 2). To allow the fit to converge quickly we cannot have too many bins in the overall ΔE-m_{ES} plane. Hence the bins outside the signal-enhanced region will have a larger size. The actual size is dictated by the need to have a good description of the smooth backgrounds. The parameters of the fit are the scaling factors of the MC PDFs, *i.e.*, the factors used to adjust the number of events in a PDF to minimize the χ^2 value of the fit.

Given the sufficient number of events for the $B^0 \to \pi^-\ell^+\nu$ and combined $B \to \pi\ell^+\nu$ decay modes, the data samples can be subdivided in 12 bins of q^2 for the signal and two bins for each of the five background categories. The use of two bins for each background component allows the fit to adjust for inaccuracies in the modelling of the shape of the background q^2 spectra. The boundaries of the two background bins of q^2 for the $B^0 \to \pi^-\ell^+\nu$ and $B \to \pi\ell^+\nu$ decays are: [0-18-26.4] GeV^2 for the $b \to u\ell\nu$ same-B category, [0-22-26.4] GeV^2 for the $b \to u\ell\nu$ both-B category, [0-10-26.4] GeV^2 for the other $B\bar{B}$ same-B category, [0-14-26.4] GeV^2 for the other $B\bar{B}$ both-B category and [0-22-26.4] GeV^2 for the continuum category. In each case, the q^2 ranges of the two bins are chosen to contain a similar number of events. In the fit to the data, we determine for each bin of q^2, the signal yield, the $b \to u\ell\nu$, the other $B\bar{B}$ and the continuum background yields in each bin of ΔE-m_{ES}.

TABLE I: Categories and number of fit parameters for each decay mode.

Categories	Decay mode				
	$\pi^-\ell\nu$ $\pi\ell\nu$	$\pi^0\ell\nu$	$\omega\ell\nu$	$\eta\ell\nu$ ($\gamma\gamma$) $\eta\ell\nu$ ($\gamma\gamma$ & 3π)	$\eta'\ell\nu$ ($\gamma\gamma$) $\eta\ell\nu$ (3π)
Signal	12	11	5	5	1
$b \to u\ell\nu$ same B	2	1	1	fixed	fixed
$b \to u\ell\nu$ both B	2	1			
other $B\bar{B}$ same B	2	1	1	1	1
other $B\bar{B}$ both B	2	1			
Continuum	2	1	1	1	fixed

Note, however, that the scaling factors obtained for each background are constrained to have the same value over their ranges of q^2 defined above. We thus have a total of 22 parameters and $(12\times34-22)$ degrees of freedom in the fit to the $B^0 \to \pi^-\ell^+\nu$ data and to the combined $B \to \pi\ell^+\nu$ data. The limited number of events for the other signal modes reduces the number of parameters, and hence the number of q^2 bins, that can be used for the fits to converge. Table I shows the number of bins of q^2 used for each signal mode as a function of the fit category.

As an initial estimate in the fit, the MC continuum background yield and q^2-dependent shape are first normalized to match the yield and q^2-dependent shape of the off-resonance data control sample. This results in a large statistical uncertainty due to the small number of events in the off-resonance data. To improve the statistical precision, the continuum background is allowed to vary in the fit to the data for the $\pi\ell\nu$, $\omega\ell\nu$ and $\eta\ell\nu(\gamma\gamma)$ modes where we have a relatively large number of events. The fit result is compatible with the measured distribution of off-resonance data. Whenever a background is not varied in the fit, it is fixed to the MC prediction, except for the continuum background which is fixed to its normalized yield and q^2-dependent shape using the off-resonance data. The background parameters which are free in the fit, typically require an adjustment of less than 10% with respect to the MC predictions. The initial agreement between MC and data is already good before we do any fit. After the fit, the agreement becomes excellent, as can be seen in Fig. 3 for a number of variables

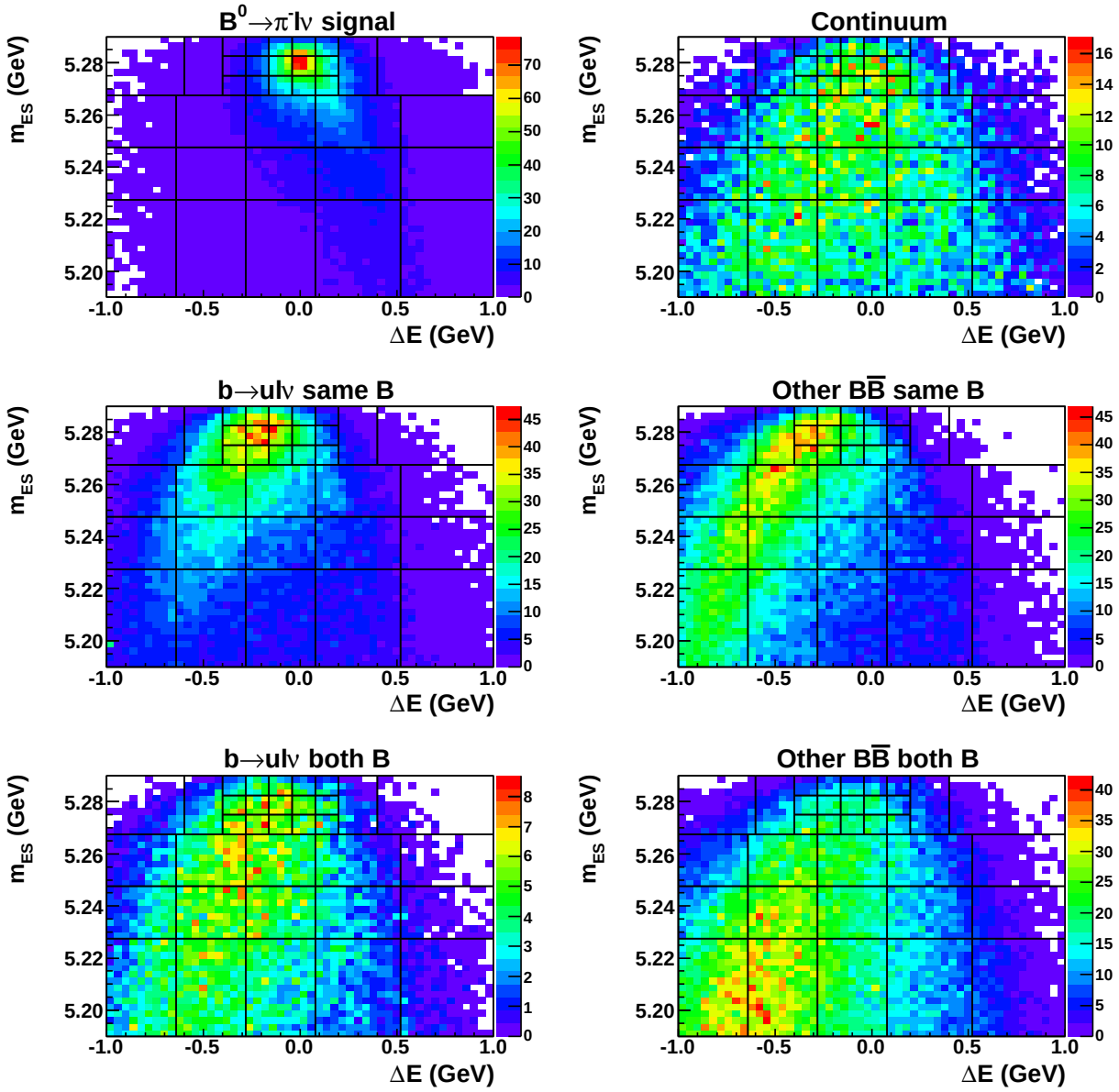

FIG. 2: (color online) ΔE-m_{ES} MC distributions, summed over all bins of q^2, for the six categories of events used in the signal extraction fit, after all the selections have been applied, in the case of the $B^0 \to \pi^- \ell^+ \nu$ decay channel. Also shown is the binning used for this decay mode.

TABLE II: Fitted yields in the full q^2 range investigated for the signal and each background category, total fitted yield and experimental data events, and values of χ^2 for the overall fit region.

Decay mode	$\pi^-\ell^+\nu$	$\pi^0\ell^+\nu$	$\pi\ell^+\nu$	$\omega\ell^+\nu$	$\eta\ell^+\nu$	$\eta'\ell^+\nu$
Signal	9297 ± 316	3204 ± 170	12448 ± 361	1861 ± 233	867 ± 101	141 ± 49
$b \to u\ell\nu$	15689 ± 664	7810 ± 334	23284 ± 796	3246 ± 293	$2411(fixed)$	$242(fixed)$
Other $B\bar{B}$	44248 ± 656	10795 ± 307	55350 ± 777	8778 ± 246	11167 ± 187	2984 ± 87
Continuum	9159 ± 459	4173 ± 236	13283 ± 537	2776 ± 270	2505 ± 155	$493(fixed)$
Fitted yield	78393 ± 507	25982 ± 228	104365 ± 531	16661 ± 172	16950 ± 153	3860 ± 71
Data events	78387 ± 280	25977 ± 161	104364 ± 323	16662 ± 129	16901 ± 130	3857 ± 62
χ^2/ndf	385.3/386	324.9/358	387.7/386	74.9/87	100.1/88	16.8/17

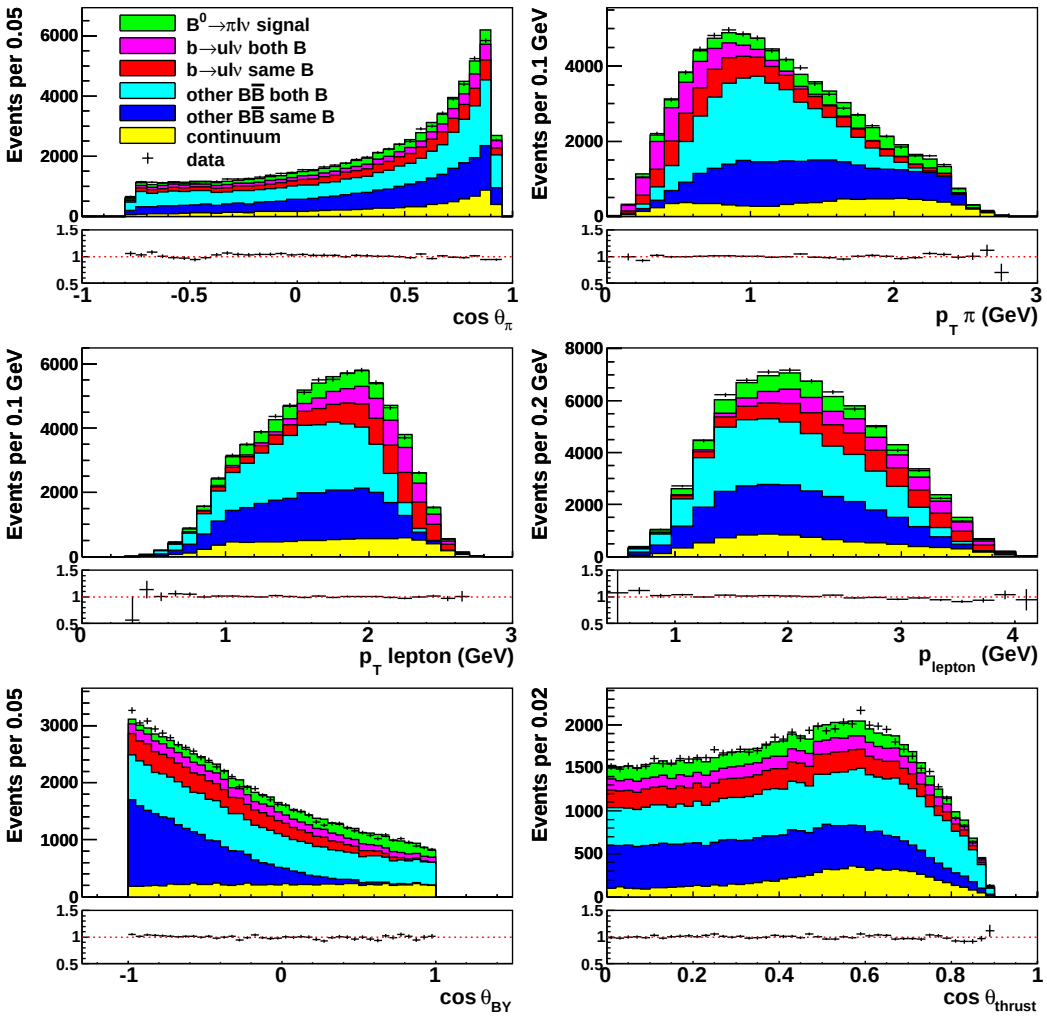

FIG. 3: (color online) Comparison of the on-resonance data and MC simulation, for $B^0 \to \pi^- \ell^+ \nu$ decays, after all analysis cuts and MC simulation corrections have been applied. The Y signal candidates related distributions are generated from events in the ΔE and m_{ES} plane with the signal-enhanced region removed. The ratios of data/MC events are presented below each panel. The general level of agreement is better than 5%.

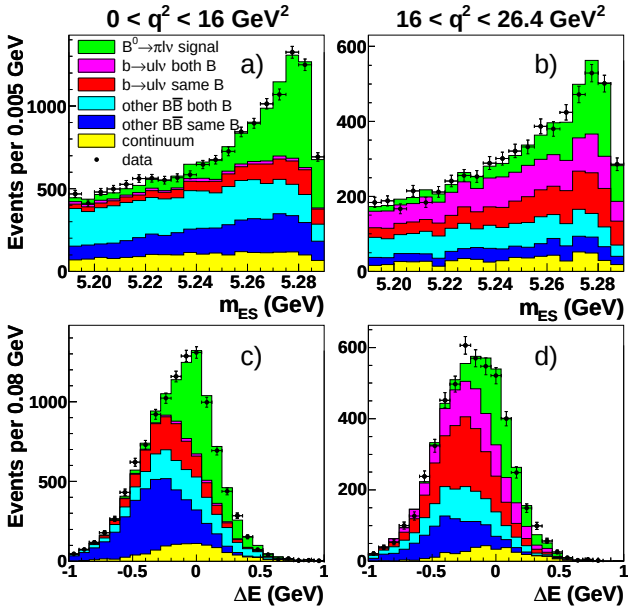

FIG. 4: (color online) Projections of the data and fit results for the $B^0 \to \pi^- \ell^+ \nu$ decays, in the signal-enhanced region: (a,b) m_{ES} with $-0.16 < \Delta E < 0.20$ GeV; and (c,d) ΔE with $m_{ES} > 5.268$ GeV. The distributions (a,c) and (b,d) are projections for $q^2 < 16$ GeV^2 and for $q^2 > 16$ GeV^2, respectively.

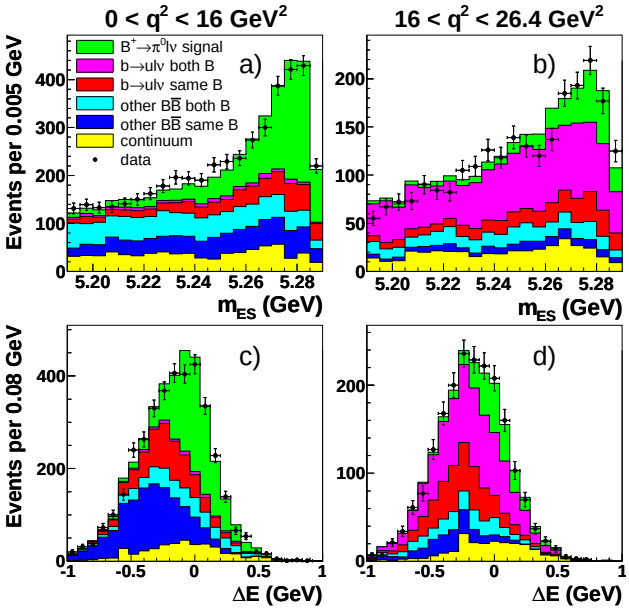

FIG. 5: (color online) Projections of the data and fit results for the $B^+ \to \pi^0 \ell^+ \nu$ decays, in the signal-enhanced region: (a,b) m_{ES} with $-0.16 < \Delta E < 0.20$ GeV; and (c,d) ΔE with $m_{ES} > 5.268$ GeV. The distributions (a,c) and (b,d) are projections for $q^2 < 16$ GeV^2 and for $q^2 > 16$ GeV^2, respectively.

of interest. The values of the scaling factors, obtained in this work, are presented in Table XIV of the Appendix for each decay channel. The full correlation matrices of the fitted scaling factors are given in Tables XV-XXII of the Appendix.

We refit the data on several different subsets obtained by dividing the final data set based on time period, electron or muon candidates, by modifying the q^2, ΔE or m_{ES} binnings, and by varying the event selections. We obtain consistent results for all subsets. We have also used MC simulation to verify that the nonresonant decay contributions to the resonance yields are negligible. For example, we find that there are 30 nonresonant $\pi^+\pi^-\pi^0\ell\nu$ events out of a total yield of 1861 ± 233 events for the $B^+ \to \omega\ell^+\nu$ decay channel.

For illustrative purposes only, we show in Figs. 4, 5, and 6, ΔE and m_{ES} fit projections in the signal-enhanced region for the $B^0 \to \pi^-\ell^+\nu$, $B^+ \to \pi^0\ell^+\nu$ and combined $B^0 \to \pi^-\ell^+\nu$ and $B^+ \to \pi^0\ell^+\nu$ decays, respectively, in two ranges of q^2 corresponding to the sum of eight bins below and four bins above $q^2 = 16$ GeV^2, respectively. More detailed ΔE and m_{ES} fit projections in each q^2 bin are shown in Figs. 13 and 14 of the Appendix for the combined $B \to \pi\ell^+\nu$ decays. The data and the fit results are in good agreement. Fit projections for $B^+ \to \omega\ell^+\nu$ and $B^+ \to \eta^{(\prime)}\ell^+\nu$ decays, over their q^2 ranges of investigation, are shown in Fig. 7. Table II gives the fitted yields in the full q^2 range studied for the signal and each background category as well as the χ^2 values and degrees of freedom for the overall fit region. The yield values in the $B^+ \to \eta\ell^+\nu$ column are the result of the fit to the combined $\gamma\gamma$ and 3π modes.

V. SYSTEMATIC UNCERTAINTIES

Systematic uncertainties on the values of the partial branching fractions, $\Delta\mathcal{B}(q^2)$, and their correlations among the q^2 bins have been investigated. These uncertainties are estimated from the variations of the resulting partial BF values (or total BF values for $B^+ \to \eta'\ell^+\nu$ decays) when the data are reanalyzed by reweighting different simulation parameters such as BFs and form factors. For each parameter, we use the full MC dataset to produce new ΔE-m_{ES} distributions ("MC event samples") by reweighting the parameter randomly over a complete Gaussian distribution whose standard deviation is given by the uncertainty on the parameter under study. One hundred such samples are produced for each parameter. Each MC event sample is analyzed the same way as real data to determine values of $\Delta\mathcal{B}(q^2)$ (or total BF values for $B^+ \to \eta'\ell^+\nu$ decays). The contribution of the parameter to the systematic uncertainty is given by the RMS value of the distribution of these $\Delta\mathcal{B}(q^2)$ values over the one hundred samples.

The systematic uncertainties due to the imperfect description of the detector in the simulation are computed by using the uncertainties determined from control samples. These include the tracking efficiency of all charged particle tracks, the particle identification efficiencies of signal candidate tracks, the calorimeter efficiencies (varied separately for photons and K_L^0), the energy deposited

TABLE III: Values of signal yields, $\Delta\mathcal{B}(q^2)$ and their relative uncertainties (%) for $B^0 \to \pi^-\ell^+\nu$ and $B^+ \to \pi^0\ell^+\nu$ decays.

Decay mode	$\pi^-\ell^+\nu$				$\pi^0\ell^+\nu$			
q^2 range (GeV^2)	q^2<12	q^2<16	q^2>16	$0 < q^2 < 26.4$	q^2<12	q^2<16	q^2>16	$0 < q^2 < 26.4$
Unfolded yield	5604.1	6982.4	2314.2	9296.5	2231.7	2666.7	537.3	3204.1
$\Delta\mathcal{B}(q^2)$ (10^{-4})	0.83	1.07	0.40	1.47	0.46	0.61	0.16	0.77
Statistical error	4.3	3.8	6.7	3.5	6.6	5.3	17.8	5.7
Detector effects	3.4	3.5	3.2	2.8	2.9	2.8	3.0	2.6
Continuum bkg	0.4	0.4	1.4	0.4	1.2	0.8	7.1	1.1
$b \to u\ell\nu$ bkg	1.6	1.4	2.1	1.3	1.7	1.5	5.9	1.9
$b \to c\ell\nu$ bkg	0.6	0.5	0.6	0.5	0.6	0.4	1.0	0.4
Other effects	2.2	2.1	2.1	2.1	2.1	2.1	2.5	2.0
Total uncertainty	6.2	5.8	8.1	5.1	7.9	6.5	20.4	6.9

TABLE IV: Values of signal yields, $\Delta\mathcal{B}(q^2)$ and their relative uncertainties (%) for combined $B \to \pi\ell^+\nu$, $B^+ \to \omega\ell^+\nu$, combined $B^+ \to \eta\ell^+\nu$ ($\gamma\gamma$ and 3π decay channels) and $B^+ \to \eta'\ell^+\nu$ decays.

Decay mode	combined $\pi\ell^+\nu$				$\omega\ell^+\nu$	$\eta\ell^+\nu$	$\eta'\ell^+\nu$
q^2 range (GeV^2)	q^2<12	q^2<16	q^2>16	$0 < q^2 < 26.4$	$0 < q^2 < 20.2$	$0 < q^2 < 22.4$	$0 < q^2 < 18.7$
Unfolded yield	7805.4	9618.9	2829.0	12447.9	1860.8	867.3	141.1
$\Delta\mathcal{B}(q^2)$ (10^{-4})	0.83	1.08	0.37	1.45	1.19	0.38	0.24
Statistical error	3.6	3.2	5.8	3.0	13.0	13.7	34.9
Detector effects	3.7	3.8	3.5	3.1	3.9	9.8	7.7
Continuum bkg	0.4	0.6	3.3	0.6	3.2	-	5.8
$b \to u\ell\nu$ bkg	1.6	1.4	4.0	1.4	5.1	8.4	4.9
$b \to c\ell\nu$ bkg	0.4	0.4	0.4	0.3	1.0	2.1	3.3
Other effects	1.8	1.7	1.5	1.6	1.8	1.8	2.4
Total uncertainty	5.8	5.5	8.7	4.9	15.0	19.0	36.7

in the calorimeter by K^0_L mesons as well as their production spectrum. The reconstruction of these neutral particles affects the analysis through the neutrino reconstruction used to obtain the values of ΔE and m_{ES}.

The uncertainties due to the generator-level inputs to the simulation are given by the uncertainties in the BFs of the background $b \to u\ell\nu$ and $b \to c\ell\nu$ processes, in the BFs of the secondary decays producing leptons, and in the BFs of the $\Upsilon(4S) \to B\bar{B}$ decays [12]. The $B \to X\ell\nu$ form-factor uncertainties, where $X = (\pi, \rho, \omega, \eta^{(\prime)}, D, D^*, D^{**})$, are given by recent calculations or measurements [12]. The uncertainties in the heavy quark parameters used in the simulation of nonresonant $b \to u\ell\nu$ events are given in Ref. [28]. The uncertainty due to final state radiation (FSR) corrections calculated by PHOTOS [29] is given by 20% [30] of the difference in the values of the BF obtained with PHOTOS switched on and with PHOTOS switched off. The uncertainty due to the modelling of the continuum is obtained by comparing the shape of its q^2 distribution to that of the off-resonance data control sample. When the continuum is fixed in the fit, the uncertainty in the total yield is used instead. The uncertainty in that case is given by the comparison of the MC total yield to the one measured off-resonance. Finally, the uncertainty due to B counting has been established to be 0.6% in *BABAR*.

Additional details on the various sources of systematic uncertainties considered in this analysis are presented in Ref. [8]. The individual sources are, to a good approximation, uncorrelated. Their associated contributions to the uncertainties can therefore be added in quadrature to yield the total systematic uncertainties for each decay mode.

The list of all the systematic uncertainties, as well as their values for the partial and total BFs, are given in Tables XXIII-XXVII of the Appendix. The term "Signal MC stat error" in these tables incorporates the systematic uncertainty due to the unfolding procedure. The correlation matrices obtained in the measurement of the partial BFs are presented in Tables XXVIII-XXXV. Condensed versions of all the uncertainties, together with signal yields and partial BFs in selected q^2 ranges, are given in Table III for the $B^0 \to \pi^-\ell^+\nu$ and $B^+ \to \pi^0\ell^+\nu$ decays, and in Table IV for the combined $B \to \pi\ell^+\nu$ decays, as well as for the $B^+ \to \omega\ell^+\nu$ and $B^+ \to \eta^{(\prime)}\ell^+\nu$ decays. The values given for the $B^+ \to \eta\ell^+\nu$ decays are

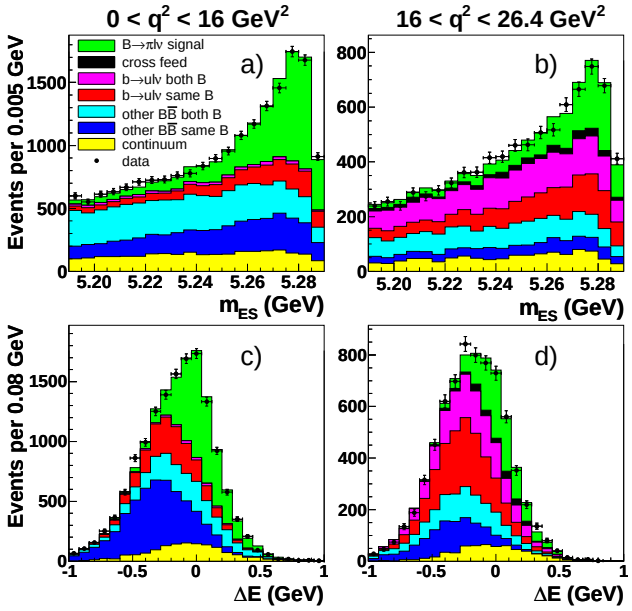

FIG. 6: (color online) Projections of the data and fit results for the combined $B^0 \to \pi^- \ell^+ \nu$ and $B^+ \to \pi^0 \ell^+ \nu$ decays, in the signal-enhanced region: (a,b) m_{ES} with $-0.16 < \Delta E < 0.20$ GeV; and (c,d) ΔE with $m_{ES} > 5.268$ GeV. The distributions (a,c) and (b,d) are projections for $q^2 < 16$ GeV^2 and for $q^2 > 16$ GeV^2, respectively.

TABLE V: Values of the total branching fractions obtained in this analysis and previous results. The two uncertainties are statistical and systematic, respectively. All BF values are $\times 10^{-4}$.

Decay mode	This analysis	Previous results	Ref.
$B \to \pi \ell^+ \nu$	$1.45 \pm 0.04 \pm 0.06$	$1.41 \pm 0.05 \pm 0.07$	[8]
$B^0 \to \pi^- \ell^+ \nu$	$1.47 \pm 0.05 \pm 0.06$	$1.44 \pm 0.06 \pm 0.07$	[8]
		$1.42 \pm 0.05 \pm 0.07$	[9]
		$1.49 \pm 0.04 \pm 0.07$	[10]
$B^+ \to \pi^0 \ell^+ \nu$	$0.77 \pm 0.04 \pm 0.03$	$0.76 \pm 0.06 \pm 0.06$	[8]
$B^+ \to \omega \ell^+ \nu$	$1.19 \pm 0.16 \pm 0.09$	$1.21 \pm 0.14 \pm 0.10$	[11]
$B^+ \to \eta \ell^+ \nu$	$0.38 \pm 0.05 \pm 0.05$	$0.36 \pm 0.05 \pm 0.04$	[9]
$B^+ \to \eta' \ell^+ \nu$	$0.24 \pm 0.08 \pm 0.03$	$0.24 \pm 0.08 \pm 0.03$	[9]

those obtained from the combined fit to the distributions of the $\eta \to \gamma\gamma$ and $\eta \to \pi^+\pi^-\pi^0$ channels. The ranges of q^2 delimited by the numbers 12, 16 are ranges used in theoretical predictions. We also give the results for the fully allowed kinematical range of q^2.

VI. BRANCHING FRACTION RESULTS

The total BF for the $B^+ \to \eta' \ell^+ \nu$ decays and the partial BFs for the other four decay modes are calculated using the unfolded signal yields, the signal efficiencies given by the simulation and the branching fractions $\mathcal{B}(\Upsilon(4S) \to B^0 \bar{B}^0) = 0.484 \pm 0.006$ and $\mathcal{B}(\Upsilon(4S) \to B^+ B^-) = 0.516 \pm 0.006$ [12]. The values of the total BF obtained in this work are compared in Table V to those reported recently.

The BFs for the $B^+ \to \eta' \ell^+ \nu$ and $B^+ \to \eta \ell^+ \nu$ decays are consistent with those presented in our earlier work [9] even though there are significant differences between the two analyses. We now use updated BFs and form-factor shapes; we have tightened various selections; we have subdivided the data in five signal bins for the $B^+ \to \eta \ell^+ \nu$ decays compared to the previous three bins; and we have also investigated the full kinematically allowed ranges of q^2 whereas this range was earlier restricted to less than 16 GeV^2 due to the very large backgrounds at high q^2. Thus, the present BF values supersede the earlier ones [9]. It should be noted that the total BF value for the $B^+ \to \eta' \ell^+ \nu$ decays has a significance of 3.2σ when we take into account only the statistical uncertainty [31]. Taking into account the effect of the systematic uncertainty which increases the total uncertainty by about 3% leads to a reduced significance of 3.1σ. We find that the total BF of the $B^+ \to \eta \ell^+ \nu$, $\eta \to \gamma\gamma$ decays ($(0.36 \pm 0.06 \pm 0.05) \times 10^{-4}$) is compatible with the total BF measured for the $B^+ \to \eta \ell^+ \nu$, $\eta \to \pi^+\pi^-\pi^0$ decays ($(0.46 \pm 0.10 \pm 0.05) \times 10^{-4}$). The total BF value in Table V for $B^+ \to \eta \ell^+ \nu$ decays is obtained from a fit to the combined $\gamma\gamma$ and 3π decay channels. This value is in good agreement with the weighted average of the total BFs obtained separately for these two decay channels.

The present BF value for $B^+ \to \omega \ell^+ \nu$ decays is in good agreement with our previous result [11], as shown in Table V. In the present analysis, we have a larger number of $\omega \ell \nu$ events (1861 ± 233 compared to 1125 ± 131 in Ref. [11]) and a better signal/background ratio (12.6% versus 9.4%). We now have a slightly larger statistical uncertainty because some of the backgrounds were previously fixed while we now fit them to the data. On the other hand, this different treatment of the backgrounds leads to a smaller systematic uncertainty in the present case. Another difference arises in the treatment of the combinatoric background, which is subtracted in Ref. [11] using a fit to the mass sideband data, while it is part of the likelihood fit in the present study. The other important difference is the use of q^2 bins of equal width in this analysis compared with varied bin width in Ref. [11]. In addition, our yields are unfolded to correct for the reconstruction effects on the measured values of q^2. The results obtained in this work use the same dataset as those of Ref. [11] but use a different analysis strategy and selection as indicated. This results in a small (estimated to be 14%) statistical overlap between the samples and a different sensitivity to sources of systematic uncertainty (estimated correlation of 75%). Since the choice of q^2 binning differs between the two analyses, only the total branching fractions can be combined. Accounting for the major sources of correlation between the measurements, the combined $\mathcal{B}(B^+ \to \omega \ell^+ \nu)$ result is: $(1.20 \pm 0.11 \pm 0.09) \times 10^{-4}$.

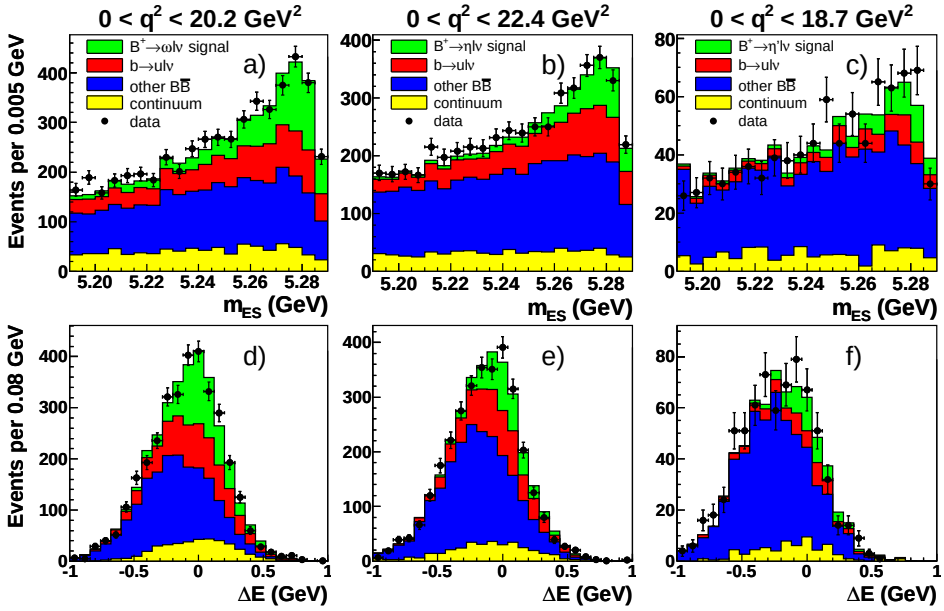

FIG. 7: (color online) Projections of the data and fit results for the $B^+ \to \omega\ell^+\nu$ and $B^+ \to \eta^{(\prime)}\ell^+\nu$ decays, in the signal-enhanced region: (a,b,c) m_{ES} with $-0.16 < \Delta E < 0.20$ GeV; and (d,e,f) ΔE with $m_{ES} > 5.268$ GeV. The distributions (a,d), (b,e) and (c,f) are projections for the $B^+ \to \omega\ell^+\nu$, combined $B^+ \to \eta\ell^+\nu$, and $B^+ \to \eta'\ell^+\nu$ decays, respectively.

Table V lists the fitted branching fractions for $B^0 \to \pi^-\ell^+\nu$, $B^+ \to \pi^0\ell^+\nu$ and the combined $B \to \pi\ell^+\nu$ modes. The $B^+ \to \pi^0\ell^+\nu$ result is used to confirm the $B^0 \to \pi^-\ell^+\nu$ result, using the isospin symmetry relation:

$$\begin{aligned}\mathcal{B}(B^0 \to \pi^-\ell^+\nu) &= \mathcal{B}(B^+ \to \pi^0\ell^+\nu) \times 2\frac{\tau_0}{\tau_+} \\ &= (1.43 \pm 0.08 \pm 0.06) \times 10^{-4}\end{aligned}$$

where $\tau_+/\tau_0 = 1.079 \pm 0.007$ [12] is the ratio of the lifetimes of B^+ and B^0 decays. The value of the branching fraction thus obtained is compatible with the BF value obtained directly for the $B^0 \to \pi^-\ell^+\nu$ decays (see Table V). The combined $B \to \pi\ell^+\nu$ decays result is based on the use of all $\pi\ell\nu$ decay events where the neutral pion events in a given q^2 bin are converted into equivalent charged pion events assuming the above isospin symmetry relation to hold for the total yield in each q^2 bin. Using these combined events leads to a smaller statistical uncertainty on the BF value.

The values of the present total BFs for the combined $B \to \pi\ell^+\nu$ decays, the $B^0 \to \pi^-\ell^+\nu$ decays and the $B^+ \to \pi^0\ell^+\nu$ decays are seen to be in good agreement with those reported earlier by *BABAR*, [8, 9] and Belle [10]. However, the present values are based on updated values of BFs and form-factor shapes, and a larger data set compared to the earlier works [8, 9]. In particular, we now have an improved model for the hybrid MC [28] distributions that describe the combination of resonant and nonresonant $b \to u\ell\nu$ decays. This model entails the use of the BGL parametrization for the $B \to \pi\ell^+\nu$ decays [9], the Ball parametrization for the $B^+ \to \omega\ell^+\nu$ decays and the BK parametrization for the $B^+ \to \eta^{(\prime)}\ell^+\nu$ decays, rather than the much older ISGW2 [32] parametrization. The use of this model leads to an increase of 3.5% in the total BF value for the $B^0 \to \pi^-\ell^+\nu$ decays, going from a value of 1.42×10^{-4} as established earlier [9] to the present value of 1.47×10^{-4}. This increase of 3.5% is significant in view of the total uncertainty of 5.1% obtained in the measurement of the total BF. Thus, the present values of BF for $B \to \pi\ell^+\nu$, $B^0 \to \pi^-\ell^+\nu$ and $B^+ \to \pi^0\ell^+\nu$ decays supersede the earlier results [8, 9].

The experimental $\Delta\mathcal{B}(q^2)$ distributions are displayed in Fig. 8 for the $B^0 \to \pi^-\ell^+\nu$ decays and for the $B^+ \to \pi^0\ell^+\nu$ decays, where each point in the $B^+ \to \pi^0\ell^+\nu$ distribution has been normalized assuming isospin symmetry to hold. The two distributions are compatible. We show the $\Delta\mathcal{B}(q^2)$ distributions in Fig. 9 for the combined $B \to \pi\ell^+\nu$ decays, in Fig. 10 for the $B^+ \to \omega\ell^+\nu$ decays, and in Fig. 11 for the $B^+ \to \eta\ell^+\nu$ decays, together with theoretical predictions. To allow a direct comparison with the theoretical predictions, which do not include FSR effects, the experimental distributions in these figures have been obtained with the efficiency "without FSR". This efficiency is given by the ratio of the total number of unfolded signal events remaining after all the cuts, from a simulation which includes FSR, to the total number of events before any cut, generated with a simulation with no FSR effects, *i.e.*, with PHOTOS switched off.

We obtain the $f_+(q^2)$ shape from a fit to these $\Delta\mathcal{B}(q^2)$ distributions. For all decays, the χ^2 function minimized in the fit to the $f_+(q^2)$ shape uses the BGL parametrization [17]. Only the $\pi\ell\nu$ decays have a sufficient number of events to warrant the use of a two-parameter polynomial expansion where values of $|V_{ub}f_+(0)|$ can be obtained from the fit extrapolated to $q^2 = 0$. For $\omega\ell\nu$ and

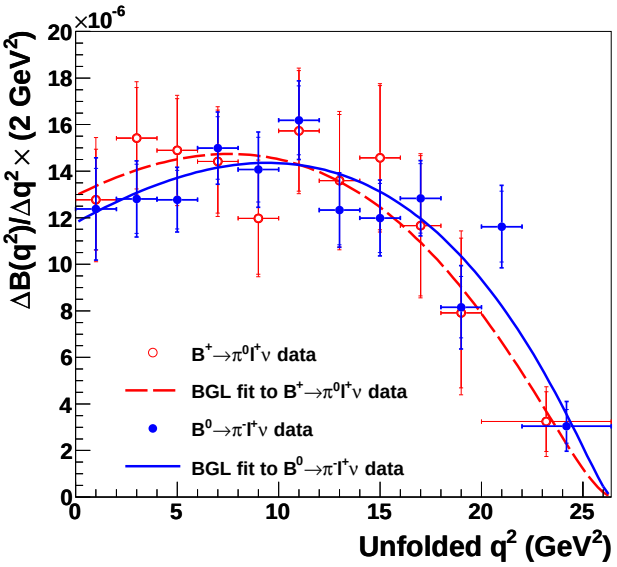

FIG. 8: (color online) Partial $\Delta\mathcal{B}(q^2)$ spectra in 12 bins of q^2 for $B^0 \to \pi^-\ell^+\nu$ and 11 bins of q^2 for $B^+ \to \pi^0\ell^+\nu$ decays. The data points are placed in the middle of each bin whose width is defined in Table XXIV.The smaller error bars are statistical only while the larger ones also include systematic uncertainties. The solid blue curve shows the result of the fit to the $B^0 \to \pi^-\ell^+\nu$ data of the BGL [17] parametrization while the dashed red curve shows the result of the fit to the $B^+ \to \pi^0\ell^+\nu$ data of the same parametrization.

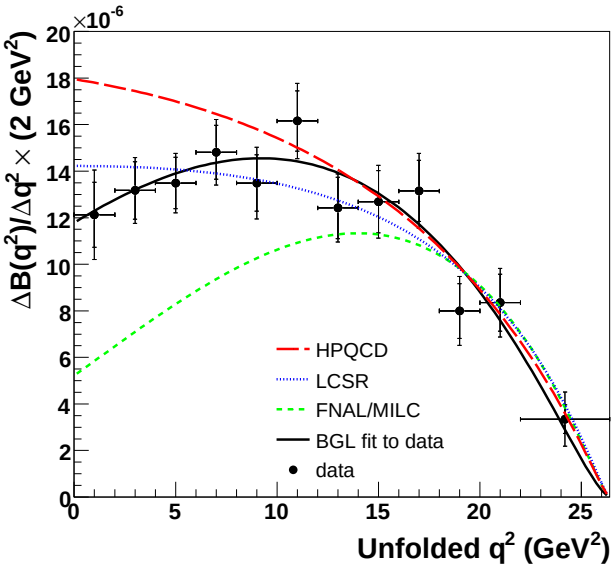

FIG. 9: (color online) Partial $\Delta\mathcal{B}(q^2)$ spectrum in 12 bins of q^2 for $B \to \pi\ell^+\nu$ decays. The data points are placed in the middle of each bin whose width is defined in Table XXIII.The smaller error bars are statistical only while the larger ones also include systematic uncertainties. The solid black curve shows the result of the fit to the data of the BGL [17] parametrization. The data are also compared to unquenched LQCD calculations (HPQCD [5], FNAL [6]) and a LCSR calculation [3].

$\eta\ell\nu$ decays we only use a one-parameter expansion. The resulting values of the fits are given in Table VI. The values of $|V_{ub}f_+(0)|$ can be used to predict rates of other decays such as $B \to \pi\pi$ [33].

We should note that the values of the BGL expansion parameters obtained in this work ($a_1/a_0 = -0.92 \pm 0.20$, $a_2/a_0 = -5.45 \pm 1.01$) differ somewhat from those obtained in Ref. [9] ($a_1/a_0 = -0.79 \pm 0.20$, $a_2/a_0 = -4.4 \pm 1.20$). Repeating the complete analysis with this new parametrization for the form-factor shape of the $B \to \pi\ell^+\nu$ decays results in only a slight change in $\mathcal{B}(B^+ \to \pi^0\ell^+\nu)$, going from 0.779 ± 0.044 to 0.773 ± 0.044, and no change in $\mathcal{B}(B^0 \to \pi^-\ell^+\nu)$ and $\mathcal{B}(B \to \pi\ell^+\nu)$. The values of a_k/a_0 obtained after this iteration are given in part a) of Table VI.

The q^2 distribution extracted from our data is compared in Fig. 9 to the shape of the form factors obtained from the three theoretical calculations listed in Table VII: the one based on Light Cone Sum Rules [3] for $q^2 < 12$ GeV^2, and the two based on unquenched LQCD [5, 6] for $q^2 > 16$ GeV^2. We first normalize the form-factor predictions to the experimental data by requiring the integrals of both to be the same over the q^2 ranges of validity given in Table VII for each theoretical prediction. Considering only experimental uncertainties, we then calculate the χ^2 probabilities relative to the binned data result for various theoretical predictions in their ranges of validity. These

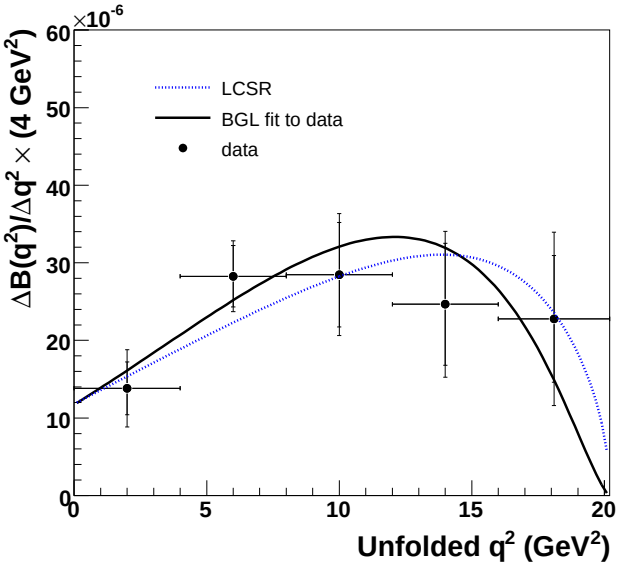

FIG. 10: (color online) Partial $\Delta\mathcal{B}(q^2)$ spectrum in 5 bins of q^2 for $B^+ \to \omega\ell^+\nu$ decays. The data points are placed in the middle of each bin whose width is defined in Table XXVI. The smaller error bars are statistical only while the larger ones also include systematic uncertainties. The data are also compared to a LCSR calculation [18].

TABLE VI: Fitted parameter values of the BGL parametrization for the exclusive semileptonic decays investigated in the present work. a) experimental data points only, fit parameters: a_0, a_1, a_2 (see Sect. VI); b) combined theoretical and experimental points, fit parameters: a_0, a_1, a_2, $|V_{ub}|$ (see Sect. VII).

Decay mode	a_1/a_0	a_2/a_0	χ^2/ndf	Prob. (%)	$\|V_{ub}f_+(0)\| \times 10^4$
a) $B^0 \to \pi^-\ell^+\nu$	-1.15 ± 0.19	-4.52 ± 1.03	9.08/9	43.0	8.7 ± 0.4
a) $B^+ \to \pi^0\ell^+\nu$	-0.63 ± 0.30	-5.80 ± 1.24	3.26/8	91.7	9.1 ± 0.5
a) $B \to \pi\ell^+\nu$	-0.93 ± 0.19	-5.40 ± 1.00	4.07/9	90.7	8.7 ± 0.3
b) $B^0 \to \pi^-\ell^+\nu$	-1.25 ± 0.20	-3.93 ± 1.19	9.24/12	68.2	8.6 ± 0.5
b) $B^+ \to \pi^0\ell^+\nu$	-1.07 ± 0.28	-3.44 ± 1.46	4.13/11	96.6	9.4 ± 0.6
b) $B \to \pi\ell^+\nu$	-1.10 ± 0.20	-4.39 ± 1.11	4.58/12	97.1	8.8 ± 0.4
$B^+ \to \omega\ell^+\nu$	-5.98 ± 0.78	-	1.54/3	67.3	-
$B^+ \to \eta\ell^+\nu$	-1.71 ± 0.87	-	0.88/3	83.1	-

TABLE VII: Values of $|V_{ub}|$ derived from the form-factor calculations (first three rows) and from the value of $|V_{ub}f_+(0)|$ (fourth row) for the combined $B \to \pi\ell^+\nu$ decays. Value of $|V_{ub}|$ derived from the form-factor calculations (last row) for the $B^+ \to \omega\ell^+\nu$ decays. The three uncertainties on $|V_{ub}|$ are statistical, systematic and theoretical, respectively. (see Sect. VII)

	q^2 (GeV^2)	$\Delta\mathcal{B}$ (10^{-4})	$\Delta\zeta$ (ps^{-1})	$\|V_{ub}\|$ (10^{-3})	χ^2/ndf	$Prob(\chi^2)$
$B \to \pi\ell^+\nu$						
HPQCD [5]	$16-26.4$	$0.37 \pm 0.02 \pm 0.02$	2.02 ± 0.55	$3.47 \pm 0.10 \pm 0.08^{+0.60}_{-0.39}$	2.7/4	60.1%
FNAL [6]	$16-26.4$	$0.37 \pm 0.02 \pm 0.02$	$2.21^{+0.47}_{-0.42}$	$3.31 \pm 0.09 \pm 0.07^{+0.37}_{-0.30}$	3.9/4	41.5%
LCSR [3]	$0-12$	$0.83 \pm 0.03 \pm 0.04$	$4.59^{+1.00}_{-0.85}$	$3.46 \pm 0.06 \pm 0.08^{+0.37}_{-0.32}$	8.0/6	24.0%
LCSR2 [34]	0			$3.34 \pm 0.10 \pm 0.05^{+0.29}_{-0.26}$		
$B^+ \to \omega\ell^+\nu$						
LCSR3 [18]	$0-20.2$	$1.19 \pm 0.16 \pm 0.09$	14.2 ± 3.3	$3.20 \pm 0.21 \pm 0.12^{+0.45}_{-0.32}$	2.24/5	81.5%

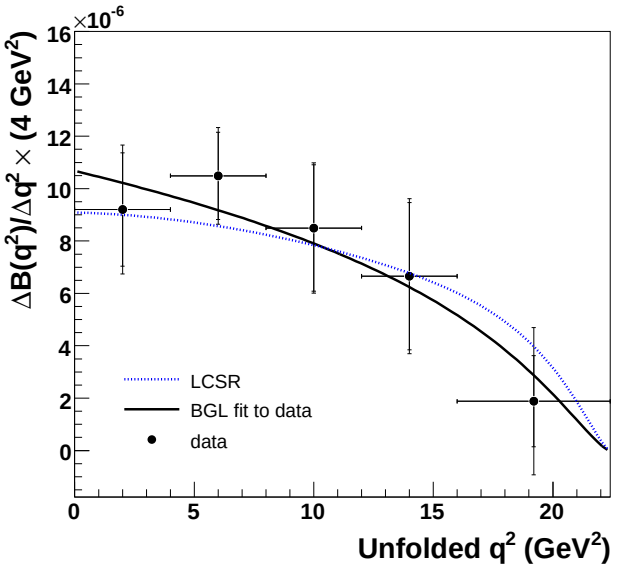

FIG. 11: (color online) Partial $\Delta\mathcal{B}(q^2)$ spectrum in 5 bins of q^2 for $B^+ \to \eta\ell^+\nu$ decays. The data points are placed in the middle of each bin whose width is defined in Table XXVII. The smaller error bars are statistical only while the larger ones also include systematic uncertainties. The data are also compared to a LCSR calculation [4].

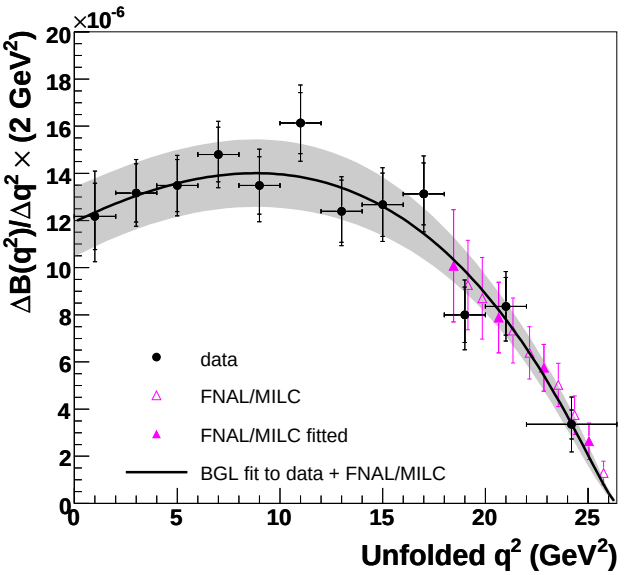

FIG. 12: (color online) Simultaneous fit of the BGL parametrization [17] to our experimental data (black solid points) and to four of the points of the FNAL/MILC predictions [6] (magenta full triangles) for the $B \to \pi\ell^+\nu$ decays. The shaded band shows the uncertainty of the fitted function. The remaining points of the FNAL/MILC predictions (magenta empty triangles) are not used in the fit.

are given in Table VII for the combined $B \to \pi\ell^+\nu$ decays. All three calculations are compatible with the data. It should be noted that the theoretical curves in Fig. 9 have been extrapolated over the full q^2 range based on the BGL parametrization obtained over their q^2 ranges of validity. These extended ranges are only meant to illustrate a possible extension of the present theoretical calculations. As shown in Figs. 10 and 11, LCSR calculations [18] and [4] are compatible with the data for the $B^+ \to \omega\ell^+\nu$ and $B^+ \to \eta\ell^+\nu$ decays, respectively.

VII. DETERMINATION OF $|V_{ub}|$

The magnitude of the CKM matrix element $|V_{ub}|$ is determined using two different approaches [6, 8].

With the first method, we extract a value of $|V_{ub}|$ from the combined $B \to \pi\ell^+\nu$ $\Delta\mathcal{B}(q^2)$ distributions using the relation:

$$|V_{ub}| = \sqrt{\Delta\mathcal{B}/(\tau_{B^0}\Delta\zeta)},$$

where $\tau_{B^0} = 1.519 \pm 0.007$ ps [12] is the B^0 lifetime and $\Delta\zeta = \Gamma/|V_{ub}|^2$ is the normalized partial decay rate predicted using the form-factor calculations [3, 5, 6]. The quantities $\Delta\mathcal{B}$ and $\Delta\zeta$ are restricted to the q^2 ranges of validity given in Table VII. The values of $\Delta\zeta$ are independent of experimental data. The values of $|V_{ub}|$ given in Table VII range from $(3.3 - 3.5) \times 10^{-3}$. These values are in good agreement with the one obtained (Table VII) from the value of $|V_{ub}f_+(0)| = (8.7 \pm 0.3) \times 10^{-4}$ measured in this work, using the value of $f_+(0) = 0.26^{+0.020}_{-0.023}$ determined in a recent LCSR calculation [34]. They are also compatible with the value of $|V_{ub}|$ determined from the $B^+ \to \omega\ell^+\nu$ data, as shown in Table VII. A value of $|V_{ub}|$ is not extracted from the $B^+ \to \eta\ell^+\nu$ decays because the theoretical partial decay rate is not sufficiently precise for these decays.

With the second method, we perform a simultaneous fit to the most recent lattice results [6] and our present experimental data to take advantage of all the available information on the form factor from the data (shape) and theory (shape and normalization).

The χ^2 function for the simultaneous fit is written as:

$$\begin{aligned}\chi^2 &= \chi^2(data) + \chi^2(lattice) \\ &= \sum_{i,j=1}^{n_{bins}} \Delta_i^{data}(V_{ij}^{data})^{-1}\Delta_j^{data} + \sum_{\ell,m=1}^{n_{points}} \Delta_\ell^{lat}(V_{\ell m}^{lat})^{-1}\Delta_m^{lat}\end{aligned}$$

where:

$$\begin{aligned}\Delta_i^{data} &= \left(\frac{\Delta\mathcal{B}}{\Delta q^2}\right)_i^{data} \\ &\quad -\frac{|V_{ub}|^2}{\Delta q_i^2}\int_{\Delta q_i^2}\frac{\tau_{B^0}G_F^2}{24\pi^3}p_\pi^3(q^2)|f_+(q^2;\alpha)|^2dq^2 \\ \Delta_\ell^{lat} &= \frac{G_F^2}{24\pi^3}p_\pi^3(q_\ell^2)\{|f_+^{lat}(q_\ell^2)|^2 - |f_+(q_\ell^2;\alpha)|^2\}\end{aligned}$$

where G_F is the Fermi constant, α denotes the set

of parameters for a chosen parametrization of $f_+(q^2)$, $\left(\Delta\mathcal{B}/\Delta q^2\right)_i^{data}$ is the measured partial BF q^2 spectrum, $|f_+^{lat}(q_\ell^2)|$ are the LQCD form-factor predictions, q_ℓ^2 is the value of q^2 for which we have a theoretical point, and $(V_{ij}^{data})^{-1}$ and $(V_{\ell m}^{lat})^{-1}$ are the inverse covariance matrices for data and theory, respectively. In our work, the function $|f_+(q_\ell^2;\alpha)|$ contains the coefficients a_k of the BGL parametrization. The result of the simultaneous fit for $B \to \pi\ell^+\nu$ decays is shown in Fig. 12, where with four theoretical points, we obtain the values of the BGL parametrization given in Table VI and $a_0 = (2.26 \pm 0.20) \times 10^{-2}$. The two values of a_k/a_0 are very similar to those obtained from a fit to the experimental data alone using the BGL parametrization. This is not surprising since the data dominate the fit. We have only used the subset with four of the 12 theoretical points in our simultaneous fit since adjacent points are very strongly correlated [6]. Alternative choices of subset give compatible results. The results shown for the $B^0 \to \pi^-\ell^+\nu$ and $B^+ \to \pi^0\ell^+\nu$ decays in Table VI are consistent with those obtained for the combined $B \to \pi\ell^+\nu$ decays.

The fit also yields: $|V_{ub}| = (3.25 \pm 0.31) \times 10^{-3}$. The previous *BABAR* result [8] of $|V_{ub}| = (2.95 \pm 0.31) \times 10^{-3}$ is about 1 standard deviation smaller. This fairly large difference can be understood from the fact the determination of $|V_{ub}|$ from the combined data-LQCD fit is most sensitive to the points at high q^2, where the changes due to the improved hybrid treatment leads to differences larger than those expected on the basis of the variation in the total BF value. The present value of $|V_{ub}|$ supersedes the one from Ref. [8].

Since the total uncertainty of 9.5% on the value of $|V_{ub}|$ results from the simultaneous fit to data and LQCD predictions, it is not so easy to identify the contributions from experiment and theory to this uncertainty. We estimate that the total uncertainty of 4.9% in the BF measurement is equivalent to an experimental uncertainty of 2.4% in the value of $|V_{ub}|$. The contribution to the uncertainty from the shape of the q^2 spectrum is determined by varying the fit parameters a_1/a_0 and a_2/a_0 within their uncertainties, and taking into account their correlation. This yields a contribution of 3.1% to the uncertainty in the value of $|V_{ub}|$. The remaining uncertainty of 8.7% arises from the form-factor normalization provided by theory.

VIII. SUMMARY

In summary, we have measured the partial BFs of $B^0 \to \pi^-\ell^+\nu$ and combined $B \to \pi\ell^+\nu$ decays in 12 bins of q^2, of $B^+ \to \pi^0\ell^+\nu$ decays in 11 bins of q^2, and of $B^+ \to \omega\ell^+\nu$ and $B^+ \to \eta\ell^+\nu$ decays in five bins of q^2. From the $B \to \pi\ell^+\nu$ distributions, we extract the $f_+(q^2)$ shapes that are found to be compatible, in the appropriate q^2 range, with all three theoretical predictions considered for these decays. LCSR calculations are also found to be consistent with our measured $B^+ \to \omega\ell^+\nu$ [18] and $B^+ \to \eta\ell^+\nu$ [4] $\Delta\mathcal{B}(q^2)$ distributions. The BGL parametrization fits our $B^0 \to \pi^-\ell^+\nu$, $B^+ \to \pi^0\ell^+\nu$ and $B \to \pi\ell^+\nu$ data well and allows us to obtain the value of $|V_{ub}f_+(0)|$. Our measured branching fractions of the five decays reported in this work lead to some improvement in our knowledge of the composition of the inclusive charmless semileptonic decay rate. In particular, the form-factor shapes are now better defined, especially for the $\pi\ell\nu$ decays. Our values of the total BF for $B^+ \to \eta^{(\prime)}\ell^+\nu$ decays are in good agreement with our earlier results [9] and supersede them. The value of the ratio $\mathcal{B}(B^+ \to \eta'\ell^+\nu)/\mathcal{B}(B^+ \to \eta\ell^+\nu) = 0.63 \pm 0.24_{stat} \pm 0.11_{syst}$ allows a significant gluonic singlet contribution to the η' form factor [4, 13]. In spite of large differences in the analysis methods for the $B^+ \to \omega\ell^+\nu$ decays, our total BF is in good agreement with our previous result [11]. The present precise value of the total BF for $B \to \pi\ell^+\nu$ decays is slightly larger than the most recent *BABAR* results [8, 9] for the reasons expounded in Sect. VI. It supersedes both results. It is in good agreement with the recent Belle result. Our value has comparable precision to the present world average [12]. For $B \to \pi\ell^+\nu$ decays, we obtain values of $|V_{ub}|$ for three different QCD calculations. The results are in good agreement with those of Refs. [8, 9]. The three values are compatible with the value of $|V_{ub}|$ obtained from our measured value of $|V_{ub}f_+(0)|$, with our value of $|V_{ub}|$ extracted from the $B^+ \to \omega\ell^+\nu$ data, and with the value of $|V_{ub}| = (3.25 \pm 0.31) \times 10^{-3}$ determined from the simultaneous fit to our experimental data and the LQCD theoretical predictions. It is compatible with the Belle result [10] of $|V_{ub}| = (3.43 \pm 0.33) \times 10^{-3}$. The tension between our values of $|V_{ub}|$ and the value of $|V_{ub}| = (4.27 \pm 0.38) \times 10^{-3}$ [12] measured in inclusive semileptonic B decays remains significant.

IX. ACKNOWLEDGMENTS

We are grateful for the extraordinary contributions of our PEP-II colleagues in achieving the excellent luminosity and machine conditions that have made this work possible. The success of this project also relies critically on the expertise and dedication of the computing organizations that support *BABAR*. The collaborating institutions wish to thank SLAC for its support and the kind hospitality extended to them. This work is supported by the US Department of Energy and National Science Foundation, the Natural Sciences and Engineering Research Council (Canada), the Commissariat à l'Energie Atomique and Institut National de Physique Nucléaire et de Physique des Particules (France), the Bundesministerium für Bildung und Forschung and Deutsche Forschungsgemeinschaft (Germany), the Istituto Nazionale di Fisica Nucleare (Italy), the Foundation for Fundamental Research on Matter (The Netherlands), the Research Council of Norway, the Ministry of Education and Science of the

Russian Federation, Ministerio de Ciencia e Innovación (Spain), and the Science and Technology Facilities Council (United Kingdom). Individuals have received support from the Marie-Curie IEF program (European Union), the A. P. Sloan Foundation (USA) and the Binational Science Foundation (USA-Israel).

X. APPENDIX

In Tables VIII-XIII, we give the functions describing the q^2 dependence of the selections used to reduce the backgrounds in the five decays under study. In Table XIV we give the values of the scaling factors obtained in our fit to the data for each decay channel. In Tables XV-XXII, we present the full correlation matrices (elements in %) of the fitting scaling factors for all the decay channels under investigation.

The list of all the systematic uncertainties, as well as their values for the partial and total BFs, are given in Tables XXIII, XXIV, XXV, XXVI and XXVII for the five decays. In Table XXIII, we have one column for each bin of q^2 and three columns for various ranges of q^2 as well as the last column for the global result. In row 1, "Fitted yield", we give the raw fitted yield as the number of events. In row 2, "Yield statistical error", we give the statistical uncertainty in % for each fitted yield. In row 3, "Unfolded yield", we give the yields from row 1 unfolded to give the true values of the yields in each bin, expressed as the number of events. In rows 4 and 6, "Efficiency", we give the efficiency in % attached to each yield. In rows 5 and 7, "Eff. (without FSR)", we give the efficiency in %, modified to remove the FSR effect. In row 8, "$\Delta\mathcal{B}$", we give the values of the partial BFs computed as usual using the true (unfolded) yields and the efficiencies with FSR. In row 9, "$\Delta\mathcal{B}$ (without FSR)", we give the values of the partial BFs computed as usual using the true (unfolded) yields and the efficiencies modified to remove the FSR effect. In rows 10 - 42, we give the contributions in % to the relative systematic uncertainties for each value of $\Delta\mathcal{B}$ as a function of q^2. In row 43, "Signal MC statistical error", we give the statistical uncertainty due to the number of MC signal events. In row 44, "Total systematic error", we give the total systematic uncertainty in % for each value of $\Delta\mathcal{B}$, obtained as the sum in quadrature of all the systematic uncertainties in each column. In row 45, "Fit error" (also denoted total statistical error), we give the statistical uncertainty in % for each value of $\Delta\mathcal{B}$ obtained from propagating the statistical uncertainties on the raw fitted yields, following the unfolding process and taking into account the efficiencies. In row 46, "Total error", we first give the total uncertainty in % for each value of $\Delta\mathcal{B}$, obtained as the sum in quadrature of the total systematic error and the fit error. We then give, in the last four columns, the total uncertainties in % for each range of q^2, obtained as the sum in quadrature of the total errors for the appropriate number of q^2 bins. A similar description applies to the other tables.

In our analysis, we compute the covariance matrix for each source of uncertainty, and use these matrices to calculate the uncertainties on the total BFs. The correlation matrices for the total statistical and systematic uncertainties are given in Tables XXVIII and XXXI for the combined $B \to \pi\ell^+\nu$ yields, in Tables XXIX and XXXII for the $B^+ \to \pi^0\ell^+\nu$ yields, in Table XXXIV for the $B^+ \to \omega\ell^+\nu$ yields and in Table XXXV for the $B^+ \to \eta\ell^+\nu$ yields. Finally, detailed ΔE and m_{ES} fit projections in each q^2 bin are also shown in Figs. 13 and 14, respectively, for the combined $B \to \pi\ell^+\nu$ decays.

TABLE VIII: q^2-dependent selections used in $B^0 \to \pi^- \ell^+ \nu$ decays.

$\cos\theta_\ell < 0.85$ for all values of q^2
$\cos\theta_\ell > 0.00000352q^{10} - 0.000235q^8 + 0.00513q^6 - 0.0383q^4 + 0.0299q^2 - 0.315$
$m^2_{miss}/2E_{miss} > -0.5$ GeV for all values of q^2
$m^2_{miss}/2E_{miss} < -0.0000499q^8 + 0.00238q^6 - 0.0342q^4 + 0.129q^2 + 0.895$ GeV
$\cos\theta_{thrust} < -0.00000578q^8 + 0.000319q^6 - 0.00737q^4 + 0.0807q^2 + 0.551$
$\theta_{miss} > 0.000829q^4 - 0.0125q^2 + 0.34$ rad
$L2 < -0.000147q^6 + 0.00141q^4 + 0.0579q^2 + 1.54$
(q^2 is given in units of GeV^2)

TABLE IX: q^2-dependent selections used in $B^+ \to \pi^0 \ell^+ \nu$ decays.

$\cos\theta_\ell < 0.9$ for all values of q^2
$\cos\theta_\ell > -0.75$, $q^2 <= 1.5$ GeV^2
$\cos\theta_\ell > 0.00000891q^{10} - 0.00057q^8 + 0.0128q^6 - 0.12q^4 + 0.456q^2 - 1.18$, $q^2 > 1.5$ GeV^2
$m^2_{miss}/2E_{miss} > -0.4$ GeV for all values of q^2
$m^2_{miss}/2E_{miss} < 0.000000167q^{10} - 0.0000448q^8 + 0.00201q^6 - 0.0315q^4 + 0.152q^2 + 0.744$ GeV
$\cos\theta_{thrust} < -0.00000146q^{10} + 0.0000679q^8 - 0.000816q^6 - 0.00298q^4 + 0.0991q^2 + 0.431$
$\theta_{miss} < 2.9$ rad for all values of q^2
$\theta_{miss} > 0.00000464q^{10} - 0.000252q^8 + 0.00474q^6 - 0.0357q^4 + 0.0996q^2 + 0.306$ rad
$L2 < -0.00000399q^{10} + 0.000199q^8 - 0.00315q^6 + 0.0127q^4 + 0.0883q^2 + 1.3$
$p^*_{lep} > 0.00000398q^{10} - 0.000251q^8 + 0.00538q^6 - 0.0459q^4 + 0.233q^2 + 0.29$ GeV
(q^2 is given in units of GeV^2)

TABLE X: q^2-dependent selections used in $B^+ \to \omega \ell^+ \nu$ decays.

$m^2_{miss}/2E_{miss} > -0.4$ GeV for all values of q^2
$m^2_{miss}/2E_{miss} < -0.00000393q^{10} + 0.0000411q^8 + 0.00305q^6 - 0.0623q^4 + 0.326q^2 + 0.49$ GeV
$\theta_{miss} < 2.65$ rad for all values of q^2
$\theta_{miss} > -0.00000244q^{10} + 0.000167q^8 - 0.00411q^6 + 0.0434q^4 - 0.173q^2 + 0.483$ rad
$L2 < -0.00000659q^{10} + 0.000316q^8 - 0.00548q^6 + 0.0381q^4 - 0.0458q^2 + 1.58$
$p^*_{lep} > -0.0000139q^{10} + 0.000929q^8 - 0.0228q^6 + 0.239q^4 - 0.838q^2 + 1.43$ GeV
$p^*_{lep} + p^*_\omega > -0.00000581q^{10} + 0.000449q^8 - 0.0129q^6 + 0.161q^4 - 0.801q^2 + 4.28$ GeV
$p^*_{\pi^0} > -0.00000479q^{10} + 0.000292q^8 - 0.00651q^6 + 0.0641q^4 - 0.278q^2 + 0.787$ GeV
(q^2 is given in units of GeV^2)

TABLE XI: q^2-dependent selections used in $B^+ \to \eta \ell^+ \nu$ ($\eta \to \gamma\gamma$) decays.

$\cos\theta_\ell < 0.9$ for all values of q^2
$\cos\theta_\ell > -0.0000582q^8 + 0.00242q^6 - 0.0302q^4 + 0.115q^2 - 0.793$
$m^2_{miss}/2E_{miss} > -0.4$ GeV for all values of q^2
$m^2_{miss}/2E_{miss} < 0.00000775q^{10} - 0.000579q^8 + 0.0152q^6 - 0.171q^4 + 0.72q^2 + 0.168$ GeV
$\cos\theta_{thrust} < -0.0000332q^8 + 0.00153q^6 - 0.0249q^4 + 0.168q^2 + 0.42$
$\theta_{miss} < 2.8$ rad for all values of q^2
$\theta_{miss} > 0.0000782q^8 - 0.00363q^6 + 0.0567q^4 - 0.32q^2 + 0.863$ rad
$p^*_{miss} < 3.2625$ GeV
$p^*_{miss} > 0.000101q^8 - 0.00456q^6 + 0.0661q^4 - 0.239q^2 + 0.819$ GeV
(q^2 is given in units of GeV^2)

TABLE XII: q^2-dependent selections used in $B^+ \to \eta\ell^+\nu$ ($\eta \to \pi^+\pi^-\pi^0$) decays.

$m^2_{miss}/2E_{miss} > -0.4$ GeV for all values of q^2
$m^2_{miss}/2E_{miss} < 0.0000082q^{10} - 0.000551q^8 + 0.0136q^6 - 0.15q^4 + 0.655q^2 + 0.0359$ GeV
$\cos\theta_{thrust} < -0.0000235q^8 + 0.00087q^6 - 0.0126q^4 + 0.0831q^2 + 0.629$
$\theta_{miss} < 2.85$ rad for all values of q^2
$\theta_{miss} > 0.0000682q^8 - 0.00298q^6 + 0.0425q^4 - 0.206q^2 + 0.595$ rad
(q^2 is given in units of GeV^2)

TABLE XIII: q^2-dependent selections used in $B^+ \to \eta'\ell^+\nu$ decays.

$m^2_{miss}/2E_{miss} > -0.3$ GeV for all values of q^2
$m^2_{miss}/2E_{miss} < 0.35q^2 + 0.325$ GeV, $q^2 < 2.5$ GeV^2
$m^2_{miss}/2E_{miss} < 1.2$ GeV, $2.5 < q^2 < 4.5$ GeV^2
$m^2_{miss}/2E_{miss} < -0.1q^2 + 1.65$ GeV, $q^2 > 4.5$ GeV^2
$\cos\theta_{thrust} < 0.05q^2 + 0.575$, $q^2 < 6.5$ GeV^2
$\cos\theta_{thrust} < 0.9$, $6.5 < q^2 < 12.5$ GeV^2
$\cos\theta_{thrust} < -0.05q^2 + 1.525$, $q^2 > 12.5$ GeV^2
$\theta_{miss} > -0.1q^2 + 0.45$ rad, $q^2 < 2.5$ GeV^2
$\theta_{miss} > 0.2$ rad, $2.5 < q^2 < 5.5$ GeV^2
$\theta_{miss} > 0.05q^2 - 0.075$ rad, $q^2 > 5.5$ GeV^2
(q^2 is given in units of GeV^2)

TABLE XIV: Values of the scaling factors given by the fit results for each decay channel. The superscripts $(u\ell\nu, 1)$ and $(u\ell\nu, 2)$ represent the $b \to u\ell\nu$ same-B and both-B backgrounds, respectively, and likewise for the other $B\bar{B}$ background.

	$\pi\ell^+\nu$	$\pi^-\ell^+\nu$	$\pi^0\ell^+\nu$	$\omega\ell^+\nu$	$\eta\ell^+\nu$	$\eta\ell^+\nu$ ($\gamma\gamma$)	$\eta\ell^+\nu$ (3π)	$\eta'\ell^+\nu$
p_1^{signal}	0.88 ± 0.09	0.89 ± 0.11	0.93 ± 0.14	0.98 ± 0.20	1.08 ± 0.23	1.20 ± 0.27	1.29 ± 0.29	1.01 ± 0.35
p_2^{signal}	0.92 ± 0.06	0.89 ± 0.07	1.05 ± 0.10	1.26 ± 0.15	1.23 ± 0.17	0.90 ± 0.19	-	-
p_3^{signal}	0.94 ± 0.05	0.90 ± 0.06	1.04 ± 0.09	1.06 ± 0.20	1.11 ± 0.26	1.12 ± 0.31	-	-
p_4^{signal}	1.00 ± 0.05	1.01 ± 0.06	0.99 ± 0.09	0.90 ± 0.21	1.01 ± 0.37	0.78 ± 0.39	-	-
p_5^{signal}	0.99 ± 0.06	1.02 ± 0.07	0.91 ± 0.11	1.02 ± 0.28	0.70 ± 0.48	0.87 ± 0.62	-	-
p_6^{signal}	1.12 ± 0.07	1.13 ± 0.08	1.08 ± 0.12	-	-	-	-	-
p_7^{signal}	1.00 ± 0.08	0.98 ± 0.09	1.09 ± 0.14	-	-	-	-	-
p_8^{signal}	1.06 ± 0.09	1.01 ± 0.10	1.18 ± 0.18	-	-	-	-	-
p_9^{signal}	1.20 ± 0.10	1.18 ± 0.11	1.11 ± 0.20	-	-	-	-	-
p_{10}^{signal}	0.97 ± 0.10	1.01 ± 0.12	0.96 ± 0.24	-	-	-	-	-
p_{11}^{signal}	1.18 ± 0.12	1.55 ± 0.17	0.89 ± 0.23	-	-	-	-	-
p_{12}^{signal}	1.19 ± 0.14	1.19 ± 0.19	-	-	-	-	-	-
$p_1^{u\ell\nu,1}$	0.65 ± 0.05	0.64 ± 0.06	0.68 ± 0.08	0.84 ± 0.08	fixed	fixed	fixed	fixed
$p_2^{u\ell\nu,1}$	0.81 ± 0.06	0.76 ± 0.06	-	-	-	-	-	-
$p_1^{u\ell\nu,2}$	1.24 ± 0.09	1.36 ± 0.12	1.17 ± 0.06	-	-	-	-	-
$p_2^{u\ell\nu,2}$	1.04 ± 0.05	1.16 ± 0.07	-	-	-	-	-	-
$p_1^{B\bar{B},1}$	0.96 ± 0.03	0.91 ± 0.03	1.13 ± 0.06	0.95 ± 0.03	0.98 ± 0.02	0.96 ± 0.03	0.96 ± 0.02	0.98 ± 0.03
$p_2^{B\bar{B},1}$	1.02 ± 0.04	1.01 ± 0.04	-	-	-	-	-	-
$p_1^{B\bar{B},2}$	0.90 ± 0.02	0.89 ± 0.02	0.90 ± 0.04	-	-	-	-	-
$p_2^{B\bar{B},2}$	1.03 ± 0.03	1.05 ± 0.03	-	-	-	-	-	-
p_1^{cont}	0.91 ± 0.04	0.90 ± 0.05	0.96 ± 0.05	1.16 ± 0.11	0.86 ± 0.05	0.88 ± 0.06	fixed	fixed
p_2^{cont}	1.08 ± 0.11	1.02 ± 0.14	-	-	-	-	-	-

TABLE XV: Correlation matrix (elements in %) of the fitted scaling factors for the $B \to \pi\ell^+\nu$ decay channel. The superscripts $(u\ell\nu, 1)$ and $(u\ell\nu, 2)$ represent the $b \to u\ell\nu$ same-B and both-B backgrounds, respectively, and likewise for the other $B\bar{B}$ background.

	p_1^π	p_2^π	p_3^π	p_4^π	p_5^π	p_6^π	p_7^π	p_8^π	p_9^π	p_{10}^π	p_{11}^π	p_{12}^π	$p_1^{u\ell\nu,1}$	$p_2^{u\ell\nu,1}$	$p_1^{u\ell\nu,2}$	$p_2^{u\ell\nu,2}$	$p_1^{B\bar{B},1}$	$p_2^{B\bar{B},1}$	$p_1^{B\bar{B},2}$	$p_2^{B\bar{B},2}$	p_1^{cont}	p_2^{cont}
p_1^π	100	27	19	8	0	3	2	5	7	11	10	1	-6	-4	13	1	24	1	18	10	-60	0
p_2^π	27	100	16	9	4	2	2	4	7	7	6	1	-9	-3	7	1	4	2	15	8	-36	0
p_3^π	19	16	100	15	12	9	10	10	12	5	5	1	-26	-9	8	3	14	18	1	5	-25	1
p_4^π	8	9	15	100	19	13	14	10	12	3	2	2	-29	-10	6	4	11	28	-17	-1	-7	2
p_5^π	0	4	12	19	100	14	16	10	11	1	0	2	-30	-11	4	5	9	32	-27	-5	2	2
p_6^π	3	2	9	13	14	100	17	9	12	2	3	1	-25	-5	0	1	19	10	-15	9	-4	1
p_7^π	2	2	10	14	16	17	100	10	14	2	5	1	-30	-4	-3	1	20	14	-14	10	-2	0
p_8^π	5	4	10	10	10	9	10	100	19	1	2	0	-31	0	1	1	18	18	4	-10	-5	0
p_9^π	7	7	12	12	11	12	14	19	100	4	13	0	-39	8	-17	-4	22	17	11	7	-9	-2
p_{10}^π	11	7	5	3	1	2	2	1	4	100	26	4	-4	-26	-4	11	11	2	6	10	-16	5
p_{11}^π	10	6	5	2	0	3	5	2	13	26	100	0	-4	3	-43	-3	9	0	11	28	-15	-1
p_{12}^π	1	1	1	2	2	1	1	0	0	4	0	100	-4	-13	9	-28	3	3	0	0	0	-34
$p_1^{u\ell\nu,1}$	-6	-9	-26	-29	-30	-25	-30	-31	-39	-4	-4	-4	100	32	-10	-9	-48	-53	-7	-16	8	-3
$p_2^{u\ell\nu,1}$	-4	-3	-9	-10	-11	-5	-4	0	8	-26	3	-13	32	100	-66	-45	-20	-26	11	6	8	-20
$p_1^{u\ell\nu,2}$	13	7	8	6	4	0	-3	1	-17	-4	-43	9	-10	-66	100	35	18	14	-12	-37	-20	16
$p_2^{u\ell\nu,2}$	1	1	3	4	5	1	1	1	-4	11	-3	-28	-9	-45	35	100	7	12	-7	-11	-1	-11
$p_1^{B\bar{B},1}$	24	4	14	11	9	19	20	18	22	11	9	3	-48	-20	18	7	100	37	4	6	-54	3
$p_2^{B\bar{B},1}$	1	2	18	28	32	10	14	18	17	2	0	3	-53	-26	14	12	37	100	-44	-39	-2	5
$p_1^{B\bar{B},2}$	18	15	1	-17	-27	-15	-14	4	11	6	11	0	-7	11	-12	-7	4	-44	100	44	-22	-3
$p_2^{B\bar{B},2}$	10	8	5	-1	-5	9	10	-10	7	10	28	0	-16	6	-37	-11	6	-39	44	100	-12	-5
p_1^{cont}	-60	-36	-25	-7	2	-4	-2	-5	-9	-16	-15	0	8	8	-20	-1	-54	-2	-22	-12	100	0
p_2^{cont}	0	0	1	2	2	1	0	0	-2	5	-1	-34	-3	-20	16	-11	3	5	-3	-5	0	100

TABLE XVI: Correlation matrix (elements in %) of the fitted scaling factors for the $B^0 \to \pi^- \ell^+ \nu$ decay channel. The superscripts $(u\ell\nu, 1)$ and $(u\ell\nu, 2)$ represent the $b \to u\ell\nu$ same-B and both-B backgrounds, respectively, and likewise for the other $B\bar{B}$ background.

	$p_1^{\pi^-}$	$p_2^{\pi^-}$	$p_3^{\pi^-}$	$p_4^{\pi^-}$	$p_5^{\pi^-}$	$p_6^{\pi^-}$	$p_7^{\pi^-}$	$p_8^{\pi^-}$	$p_9^{\pi^-}$	$p_{10}^{\pi^-}$	$p_{11}^{\pi^-}$	$p_{12}^{\pi^-}$	$p_1^{u\ell\nu,1}$	$p_2^{u\ell\nu,1}$	$p_1^{u\ell\nu,2}$	$p_2^{u\ell\nu,2}$	$p_1^{B\bar{B},1}$	$p_2^{B\bar{B},1}$	$p_1^{B\bar{B},2}$	$p_2^{B\bar{B},2}$	p_1^{cont}	p_2^{cont}
$p_1^{\pi^-}$	100	29	20	7	0	3	2	5	7	9	7	1	-6	-3	14	1	27	1	19	9	-64	1
$p_2^{\pi^-}$	29	100	16	7	3	2	2	4	6	5	5	0	-7	-2	8	1	4	1	15	8	-37	0
$p_3^{\pi^-}$	20	16	100	13	11	9	10	9	11	4	4	1	-24	-8	8	3	14	17	0	4	-26	2
$p_4^{\pi^-}$	7	7	13	100	18	12	14	10	11	2	3	1	-27	-10	5	4	9	27	-19	-3	-6	2
$p_5^{\pi^-}$	0	3	11	18	100	13	15	9	10	0	1	1	-27	-10	4	4	7	31	-28	-7	3	2
$p_6^{\pi^-}$	3	2	9	12	13	100	17	8	11	2	3	1	-24	-4	0	1	17	8	-15	9	-4	1
$p_7^{\pi^-}$	2	2	10	14	15	17	100	10	14	2	5	1	-29	-3	-3	1	18	13	-16	10	-2	0
$p_8^{\pi^-}$	5	4	9	10	9	8	10	100	19	1	2	0	-31	0	0	0	17	18	3	-11	-5	0
$p_9^{\pi^-}$	7	6	11	11	10	11	14	19	100	5	13	0	-39	9	-19	-5	20	16	11	7	-8	-2
$p_{10}^{\pi^-}$	9	5	4	2	0	2	2	1	5	100	25	3	-3	-22	-9	10	9	2	5	9	-13	5
$p_{11}^{\pi^-}$	7	5	4	2	1	3	5	2	13	25	100	0	-5	1	-41	-2	7	1	10	26	-9	-1
$p_{12}^{\pi^-}$	1	0	1	1	1	1	1	0	0	3	0	100	-3	-9	6	-27	2	3	0	0	0	-33
$p_1^{u\ell\nu,1}$	-6	-7	-24	-27	-27	-24	-29	-31	-39	-3	-5	-3	100	30	-8	-9	-44	-50	-8	-17	7	-4
$p_2^{u\ell\nu,1}$	-3	-2	-8	-10	-10	-4	-3	0	9	-22	1	-9	30	100	-65	-46	-18	-27	13	10	6	-23
$p_1^{u\ell\nu,2}$	14	8	8	5	4	0	-3	0	-19	-9	-41	6	-8	-65	100	34	18	12	-12	-38	-20	18
$p_2^{u\ell\nu,2}$	1	1	3	4	4	1	1	0	-5	10	-2	-27	-9	-46	34	100	7	12	-7	-10	-1	-11
$p_1^{B\bar{B},1}$	27	4	14	9	7	17	18	17	20	9	7	2	-44	-18	18	7	100	33	-3	5	-55	3
$p_2^{B\bar{B},1}$	1	1	17	27	31	8	13	18	16	2	1	3	-50	-27	12	12	33	100	-46	-43	-1	5
$p_1^{B\bar{B},2}$	19	15	0	-19	-28	-15	-16	3	11	5	10	0	-8	13	-12	-7	-3	-46	100	45	-22	-3
$p_2^{B\bar{B},2}$	9	8	4	-3	-7	9	10	-11	7	9	26	0	-17	10	-38	-10	5	-43	45	100	-10	-5
p_1^{cont}	-64	-37	-26	-6	3	-4	-2	-5	-8	-13	-9	0	7	6	-20	-1	-55	-1	-22	-10	100	0
p_2^{cont}	1	0	2	2	2	1	0	0	-2	5	-1	-33	-4	-23	18	-11	3	5	-3	-5	0	100

TABLE XVII: Correlation matrix (elements in %) of the fitted scaling factors for the $B^+ \to \pi^0 \ell^+ \nu$ decay channel. The superscripts $(u\ell\nu, 1)$ and $(u\ell\nu, 2)$ represent the $b \to u\ell\nu$ same-B and both-B backgrounds, respectively, and likewise for the other $B\bar{B}$ background.

	$p_1^{\pi^0}$	$p_2^{\pi^0}$	$p_3^{\pi^0}$	$p_4^{\pi^0}$	$p_5^{\pi^0}$	$p_6^{\pi^0}$	$p_7^{\pi^0}$	$p_8^{\pi^0}$	$p_9^{\pi^0}$	$p_{10}^{\pi^0}$	$p_{11}^{\pi^0}$	$p_1^{u\ell\nu,1}$	$p_1^{u\ell\nu,2}$	$p_1^{B\bar{B},1}$	$p_1^{B\bar{B},2}$	p_1^{cont}
$p_1^{\pi^0}$	100	17	13	9	5	2	1	2	5	7	4	-7	13	10	10	-43
$p_2^{\pi^0}$	17	100	13	9	6	3	3	4	6	7	3	-12	12	5	13	-32
$p_3^{\pi^0}$	13	13	100	10	9	7	6	7	8	8	1	-20	17	8	8	-23
$p_4^{\pi^0}$	9	9	10	100	11	9	8	8	8	7	-1	-21	19	11	-1	-14
$p_5^{\pi^0}$	5	6	9	11	100	12	11	10	8	7	-4	-26	23	17	-11	-6
$p_6^{\pi^0}$	2	3	7	9	12	100	10	9	7	6	-4	-22	20	16	-14	-2
$p_7^{\pi^0}$	1	3	6	8	11	10	100	9	8	7	-1	-25	16	14	-7	0
$p_8^{\pi^0}$	2	4	7	8	10	9	9	100	9	8	1	-26	13	14	0	-1
$p_9^{\pi^0}$	5	6	8	8	8	7	8	9	100	12	9	-27	6	15	7	-7
$p_{10}^{\pi^0}$	7	7	8	7	7	6	7	8	12	100	20	-23	-5	16	9	-11
$p_{11}^{\pi^0}$	4	3	1	-1	-4	-4	-1	1	9	20	100	6	-57	-4	21	-8
$p_1^{u\ell\nu,1}$	-7	-12	-20	-21	-26	-22	-25	-26	-27	-23	6	100	-55	-63	-12	10
$p_1^{u\ell\nu,2}$	13	12	17	19	23	20	16	13	6	-5	-57	-55	100	50	-25	-25
$p_1^{B\bar{B},1}$	10	5	8	11	17	16	14	14	15	16	-4	-63	50	100	-33	-35
$p_1^{B\bar{B},2}$	10	13	8	-1	-11	-14	-7	0	7	9	21	-12	-25	-33	100	-7
p_1^{cont}	-43	-32	-23	-14	-6	-2	0	-1	-7	-11	-8	10	-25	-35	-7	100

TABLE XVIII: Correlation matrix (elements in %) of the fitted scaling factors for the $B^+ \to \omega\ell^+\nu$ decay channel.

	p_1^{ω}	p_2^{ω}	p_3^{ω}	p_4^{ω}	p_5^{ω}	$p_1^{u\ell\nu}$	$p_1^{B\bar{B}}$	p_1^{cont}
p_1^{ω}	100	12	7	10	2	12	7	-46
p_2^{ω}	12	100	11	7	11	-5	-36	7
p_3^{ω}	7	11	100	19	26	-24	-3	0
p_4^{ω}	10	7	19	100	58	-59	26	-15
p_5^{ω}	2	11	26	58	100	-85	19	3
$p_1^{u\ell\nu}$	12	-5	-24	-59	-85	100	-19	-22
$p_1^{B\bar{B}}$	7	-36	-3	26	19	-19	100	-61
p_1^{cont}	-46	7	0	-15	3	-22	-61	100

TABLE XIX: Correlation matrix (elements in %) of the fitted scaling factors for the $B^+ \to \eta\ell^+\nu$ $(\gamma\gamma)$ decay channel.

	$p_1^{\eta,\gamma\gamma}$	$p_2^{\eta,\gamma\gamma}$	$p_3^{\eta,\gamma\gamma}$	$p_4^{\eta,\gamma\gamma}$	$p_5^{\eta,\gamma\gamma}$	$p_1^{B\bar{B}}$	p_1^{cont}
$p_1^{\eta,\gamma\gamma}$	100	18	1	-1	9	17	-59
$p_2^{\eta,\gamma\gamma}$	18	100	9	10	13	-17	-23
$p_3^{\eta,\gamma\gamma}$	1	9	100	12	10	-29	5
$p_4^{\eta,\gamma\gamma}$	-1	10	12	100	12	-37	11
$p_5^{\eta,\gamma\gamma}$	9	13	10	12	100	-26	-7
$p_1^{B\bar{B}}$	17	-17	-29	-37	-26	100	-45
p_1^{cont}	-59	-23	5	11	-7	-45	100

TABLE XX: Correlation matrix (elements in %) of the fitted scaling factors for the $B^+ \to \eta\ell^+\nu$ $(\pi^+\pi^-\pi^0)$ decay channel.

	$p_1^{\eta,3\pi}$	$p_1^{B\bar{B}}$
$p_1^{\eta,3\pi}$	100	-48
$p_1^{B\bar{B}}$	-48	100

TABLE XXI: Correlation matrix (elements in %) of the fitted scaling factors for the $B^+ \to \eta\ell^+\nu$ $(\gamma\gamma + 3\pi)$ decay channel.

	p_1^{η}	p_2^{η}	p_3^{η}	p_4^{η}	p_5^{η}	$p_1^{B\bar{B}}$	p_1^{cont}
p_1^{η}	100	17	1	0	7	18	-57
p_2^{η}	17	100	5	6	8	-9	-23
p_3^{η}	1	5	100	8	6	-22	3
p_4^{η}	0	6	8	100	8	-29	7
p_5^{η}	7	8	6	8	100	-19	-6
$p_1^{B\bar{B}}$	18	-9	-22	-29	-19	100	-47
p_1^{cont}	-57	-23	3	7	-6	-47	100

TABLE XXII: Correlation matrix (elements in %) of the fitted scaling factors for the $B^+ \to \eta'\ell^+\nu$ $(\gamma\gamma)$ decay channel.

	$p_1^{\eta'}$	$p_1^{B\bar{B}}$
$p_1^{\eta'}$	100	-58
$p_1^{B\bar{B}}$	-58	100

TABLE XXIII: Combined $B^0 \to \pi^- \ell^+ \nu$ and $B^+ \to \pi^0 \ell^+ \nu$ yields, efficiencies (%), $\Delta\mathcal{B}$ (10^{-7}) and their relative uncertainties (%). The $\Delta\mathcal{B}$ and efficiency values labeled "without FSR" are modified to remove FSR effects. This procedure has no significant impact on the $\Delta\mathcal{B}$ values.

q^2 bins (GeV^2)	0-2	2-4	4-6	6-8	8-10	10-12	12-14	14-16	16-18	18-20	20-22	22-26.4	q^2<12	q^2<16	q^2>16	Total
Fitted yield	849.9	1210.4	1447.3	1557.9	1374.9	1293.0	959.4	866.8	870.2	672.6	710.4	635.3	7733.2	9559.4	2888.5	12447.9
Yield statistical error	9.9	6.5	5.3	5.4	6.0	6.0	7.5	8.1	8.1	10.5	10.4	12.1	2.6	3.0	5.6	2.9
Unfolded yield	889.1	1207.8	1431.5	1581.6	1327.2	1368.2	926.5	887.0	948.3	633.9	699.5	547.3	7805.4	9618.9	2829.0	12447.9
$\pi^- \ell\nu$ Efficiency	6.18	7.39	8.52	8.38	7.94	7.00	6.45	6.13	6.34	6.79	6.77	6.06	-	-	-	-
$\pi^- \ell\nu$ Eff. (without FSR)	5.93	7.29	8.46	8.46	7.99	7.06	6.49	6.21	6.38	6.88	6.83	6.11	-	-	-	-
$\pi^0 \ell\nu$ Efficiency	4.00	5.14	5.88	6.03	5.21	4.19	3.22	2.81	2.92	3.44	4.45	3.87	-	-	-	-
$\pi^0 \ell\nu$ Eff. (without FSR)	3.95	5.15	5.92	6.05	5.24	4.19	3.22	2.80	2.93	3.45	4.41	3.85	-	-	-	-
$\Delta\mathcal{B}$	117.2	130.5	134.5	149.3	135.7	162.5	124.8	128.0	132.2	80.9	83.9	74.0	829.7	1082.5	371.0	1453.5
$\Delta\mathcal{B}$ (without FSR)	121.3	131.7	134.9	148.1	134.9	161.6	124.2	126.8	131.5	80.0	83.5	73.6	832.5	1083.5	368.6	1452.1
Tracking efficiency	4.3	1.4	1.3	2.2	2.5	1.3	1.9	1.6	1.0	0.6	3.1	2.0	2.0	2.0	1.3	1.8
Photon efficiency	5.6	2.6	1.1	3.1	3.0	3.0	2.8	3.7	2.9	4.9	3.8	16.2	2.9	3.0	2.7	2.1
K^0_L efficiency	1.5	0.3	0.3	0.5	0.5	0.3	0.5	0.6	0.9	0.6	0.6	0.5	0.4	0.4	0.4	0.4
K^0_L production spectrum	1.3	0.5	0.6	1.2	3.2	3.2	1.3	2.6	4.0	4.9	1.0	4.2	0.5	0.5	1.3	0.5
K^0_L energy	0.4	0.3	0.2	0.2	0.3	0.2	0.2	0.2	0.3	0.4	0.5	0.5	0.1	0.1	0.2	0.1
ℓ identification	0.2	1.2	1.4	1.2	1.3	0.9	1.2	1.4	1.2	1.8	1.5	0.8	1.0	1.1	1.3	1.1
π identification	0.2	0.1	0.1	0.1	0.1	0.1	0.2	0.1	0.2	0.2	0.2	0.2	0.1	0.1	0.1	0.1
Bremsstrahlung	0.2	0.1	0.1	0.1	0.2	0.1	0.1	0.1	0.1	0.3	0.2	0.3	0.1	0.1	0.2	0.1
q^2 continuum shape	7.8	2.3	2.3	1.2	2.5	1.8	1.4	2.1	2.8	6.7	4.9	15.1	0.4	0.6	3.3	0.6
$\mathcal{B}(B^0 \to \rho^- \ell^+ \nu)$	0.2	0.2	0.1	0.1	0.2	0.1	0.1	0.3	0.3	1.0	1.1	0.3	0.1	0.1	0.5	0.2
$\mathcal{B}(B^+ \to \rho^0 \ell^+ \nu)$	0.2	0.1	0.1	0.0	0.1	0.1	0.1	0.2	0.1	0.5	0.2	0.4	0.1	0.1	0.1	0.1
$\mathcal{B}(B^+ \to \omega \ell^+ \nu)$	0.2	0.1	0.0	0.0	0.1	0.0	0.1	0.1	0.2	0.3	0.2	0.7	0.1	0.1	0.3	0.1
$\mathcal{B}(B^+ \to \eta \ell^+ \nu)$	0.1	0.0	0.0	0.0	0.0	0.0	0.1	0.1	0.1	0.4	0.3	0.4	0.0	0.0	0.2	0.1
$\mathcal{B}(B^+ \to \eta' \ell^+ \nu)$	0.1	0.0	0.0	0.0	0.0	0.0	0.1	0.1	0.1	0.1	0.1	0.1	0.0	0.0	0.1	0.1
Nonresonant $b \to u\ell\nu$ BF	0.2	0.2	0.1	0.2	0.1	0.1	0.1	0.3	0.2	0.8	0.8	1.4	0.1	0.1	0.4	0.2
SF parameters	0.6	0.6	0.5	0.5	0.5	0.1	0.8	0.4	0.6	1.3	5.0	10.5	0.4	0.2	2.8	0.8
$B \to \rho\ell\nu$ FF	1.1	1.5	2.1	2.0	2.8	2.3	1.3	2.0	3.1	4.2	2.3	15.0	1.5	1.3	2.8	1.0
$B^0 \to \pi^- \ell^+ \nu$ FF	0.2	0.0	0.0	0.0	0.0	0.0	0.0	0.1	0.1	0.3	0.1	0.1	0.0	0.0	0.1	0.0
$B^+ \to \eta^{(\prime)} \ell^+ \nu$ FF	0.1	0.1	0.0	0.0	0.0	0.0	0.1	0.1	0.1	0.2	0.2	0.3	0.1	0.1	0.1	0.1
$B^+ \to \omega \ell^+ \nu$ FF	0.2	0.1	0.1	0.1	0.2	0.1	0.1	0.1	0.1	0.6	0.2	2.4	0.1	0.1	0.7	0.2
$\mathcal{B}(B \to D\ell\nu)$	0.4	0.6	0.2	0.1	0.2	0.2	0.4	0.2	0.4	0.2	0.3	0.2	0.2	0.2	0.2	0.2
$\mathcal{B}(B \to D^*\ell\nu)$	0.4	0.3	0.2	0.1	0.2	0.2	0.2	0.1	0.1	0.3	0.3	0.1	0.2	0.2	0.2	0.2
$\mathcal{B}(B \to D^{**}\ell\nu)$	0.4	0.2	0.2	0.2	0.2	0.2	0.3	0.2	0.2	0.3	0.3	0.2	0.2	0.2	0.1	0.1
Nonresonant $b \to c\ell\nu$ BF	0.6	0.3	0.3	0.2	0.2	0.2	0.2	0.3	0.2	0.4	0.2	0.1	0.2	0.2	0.1	0.1
$B \to D\ell\nu$ FF	0.2	0.1	0.2	0.1	0.3	0.1	0.1	0.1	0.2	0.3	0.3	0.1	0.1	0.1	0.1	0.1
$B \to D^*\ell\nu$ FF	0.2	0.1	0.1	0.1	0.1	0.2	0.2	0.4	0.1	0.3	0.6	0.2	0.1	0.1	0.2	0.1
$B \to D^{**}\ell\nu$ FF	0.3	0.1	0.0	0.0	0.6	0.6	0.1	0.7	0.2	0.2	0.2	0.3	0.1	0.2	0.1	0.1
$\Upsilon(4S) \to B^0\bar{B}^0$ BF	0.6	0.9	0.5	0.6	0.7	0.7	0.9	0.8	0.9	0.6	0.2	0.1	0.7	0.7	0.5	0.7
Secondary lepton	2.0	1.6	1.4	1.0	1.4	0.6	0.4	0.5	0.2	0.9	2.4	0.2	0.8	0.6	0.8	0.7
Final state radiation	0.2	1.6	1.5	1.3	1.3	1.3	1.5	1.1	1.3	0.6	1.3	0.2	1.2	1.3	0.9	1.2
B counting	0.6	0.6	0.6	0.6	0.6	0.6	0.6	0.6	0.6	0.6	0.6	0.6	0.6	0.6	0.6	0.6
B lifetimes	0.2	0.2	0.2	0.2	0.2	0.2	0.1	0.1	0.1	0.1	0.2	0.2	0.1	0.2	0.1	0.2
Fit bias	0.7	0.2	1.1	0.1	0.3	0.4	0.5	0.2	0.3	1.0	0.4	0.6	0.4	0.4	0.1	0.3
Signal MC stat error	1.3	1.4	1.2	1.3	1.2	1.3	1.5	1.4	1.3	1.5	1.2	1.4	0.5	0.4	0.6	0.3
Total systematic error	11.2	5.3	4.8	5.3	7.0	6.0	5.1	6.3	7.1	11.2	9.7	29.4	4.5	4.5	6.5	3.8
Fit error	11.5	9.4	8.2	7.8	9.0	8.0	10.6	10.6	10.0	14.7	14.7	18.4	3.6	3.2	5.8	3.0
Total error	16.1	10.8	9.5	9.5	11.4	10.0	11.8	12.3	12.2	18.5	17.6	34.7	5.8	5.5	8.7	4.9

TABLE XXIV: $B^0 \to \pi^-\ell^+\nu$ yields, efficiencies (%), $\Delta\mathcal{B}$ (10^{-7}) and their relative uncertainties (%). The $\Delta\mathcal{B}$ and efficiency values labeled "without FSR" are modified to remove FSR effects. This procedure has no significant impact on the $\Delta\mathcal{B}$ values.

q^2 bins (GeV^2)	0-2	2-4	4-6	6-8	8-10	10-12	12-14	14-16	16-18	18-20	20-22	22-26.4	q^2<12	q^2<16	q^2>16	Total
Fitted yield	630.6	846.6	992.7	1111.7	1022.7	966.0	734.1	662.3	687.2	547.0	656.8	439.0	5570.2	6966.6	2329.9	9296.5
Yield statistical error	12.2	8.2	6.5	6.3	6.9	7.1	8.9	9.6	9.7	12.0	10.7	15.9	3.1	3.6	6.5	3.4
Unfolded yield	649.8	832.6	964.3	1133.4	1003.0	1021.0	714.6	663.8	731.7	502.3	713.0	367.1	5604.1	6982.4	2314.2	9296.5
Efficiency	6.18	7.39	8.52	8.38	7.94	7.00	6.45	6.13	6.34	6.79	6.77	6.06	-	-	-	-
Eff. (without FSR)	5.93	7.29	8.46	8.46	7.99	7.06	6.49	6.21	6.38	6.88	6.83	6.11	-	-	-	-
$\Delta\mathcal{B}$	117.5	125.9	126.6	151.2	141.3	163.1	123.9	121.1	129.0	82.7	117.8	67.8	825.6	1070.6	397.3	1467.9
$\Delta\mathcal{B}$ (without FSR)	122.5	127.7	127.4	149.8	140.5	161.7	123.1	119.6	128.3	81.6	116.7	67.2	829.6	1072.3	393.8	1466.1
Tracking efficiency	4.9	1.5	1.5	2.5	3.3	2.5	1.9	3.1	2.6	9.5	4.0	14.7	2.2	2.2	2.2	1.9
Photon efficiency	5.0	1.7	0.6	2.3	3.0	2.8	2.4	3.0	1.3	9.2	4.0	17.6	2.3	2.4	1.9	1.6
K^0_L efficiency	1.4	0.5	0.3	0.4	0.7	0.4	0.6	0.5	0.6	0.5	0.7	0.9	0.4	0.4	0.4	0.4
K^0_L production spectrum	1.5	0.6	0.7	0.6	1.1	0.5	0.8	0.8	0.6	0.9	1.0	2.2	0.5	0.6	0.6	0.6
K^0_L energy	0.4	0.5	0.3	0.2	0.4	0.3	0.2	0.2	0.4	0.4	0.4	1.2	0.1	0.1	0.2	0.1
ℓ identification	0.3	1.6	1.2	1.2	1.5	0.9	1.1	1.5	1.1	2.1	0.9	0.5	1.1	1.1	1.0	1.1
π identification	0.2	0.1	0.1	0.1	0.1	0.1	0.1	0.2	0.2	0.2	0.2	0.4	0.1	0.1	0.2	0.2
Bremsstrahlung	0.2	0.1	0.2	0.1	0.2	0.1	0.1	0.1	0.1	0.2	0.1	0.5	0.1	0.1	0.2	0.1
q^2 continuum shape	7.8	2.3	1.8	0.7	0.4	0.1	0.9	0.6	1.2	3.5	2.1	0.7	0.4	0.4	1.4	0.4
$\mathcal{B}(B^+ \to \pi^0\ell^+\nu)$	0.2	0.1	0.1	0.0	0.0	0.0	0.1	0.1	0.1	0.3	0.3	1.7	0.1	0.1	0.5	0.1
$\mathcal{B}(B^0 \to \rho^-\ell^+\nu)$	0.2	0.2	0.1	0.1	0.3	0.1	0.1	0.2	0.4	0.5	0.6	1.4	0.1	0.1	0.3	0.2
$\mathcal{B}(B^+ \to \rho^0\ell^+\nu)$	0.2	0.1	0.1	0.1	0.1	0.1	0.1	0.2	0.1	0.3	0.2	1.2	0.1	0.1	0.2	0.1
$\mathcal{B}(B^+ \to \omega\ell^+\nu)$	0.2	0.1	0.1	0.1	0.0	0.1	0.1	0.1	0.1	0.4	0.2	1.4	0.1	0.1	0.4	0.1
$\mathcal{B}(B^+ \to \eta\ell^+\nu)$	0.2	0.1	0.1	0.0	0.0	0.0	0.1	0.1	0.1	0.3	0.3	0.8	0.1	0.1	0.2	0.1
$\mathcal{B}(B^+ \to \eta'\ell^+\nu)$	0.2	0.1	0.1	0.0	0.1	0.1	0.1	0.1	0.1	0.2	0.1	0.5	0.1	0.1	0.2	0.1
Nonresonant $b \to u\ell\nu$ BF	0.2	0.2	0.1	0.2	0.2	0.1	0.1	0.2	0.3	0.7	0.9	1.9	0.1	0.1	0.6	0.2
SF parameters	0.4	0.7	0.6	0.5	0.5	0.1	0.7	0.1	0.6	2.4	2.8	8.1	0.4	0.3	1.6	0.6
$B \to \rho\ell\nu$ FF	1.2	1.4	1.9	1.8	1.3	1.4	0.8	0.6	1.8	2.7	0.8	3.6	1.5	1.3	0.8	1.1
$B^0 \to \pi^-\ell^+\nu$ FF	0.3	0.1	0.1	0.0	0.1	0.0	0.1	0.1	0.1	0.3	0.0	0.7	0.1	0.1	0.2	0.1
$B^+ \to \eta^{(\prime)}\ell^+\nu$ FF	0.2	0.1	0.1	0.0	0.0	0.0	0.1	0.1	0.1	0.2	0.1	0.4	0.1	0.1	0.2	0.1
$B^+ \to \omega\ell^+\nu$ FF	0.2	0.1	0.1	0.1	0.1	0.1	0.1	0.1	0.1	0.6	0.1	3.5	0.1	0.1	0.7	0.2
$\mathcal{B}(B \to D\ell\nu)$	0.5	0.7	0.2	0.1	0.2	0.2	0.4	0.3	0.5	0.3	0.3	0.5	0.2	0.2	0.3	0.3
$\mathcal{B}(B \to D^*\ell\nu)$	0.5	0.3	0.2	0.2	0.3	0.3	0.3	0.2	0.2	0.3	0.3	0.5	0.2	0.2	0.2	0.2
$\mathcal{B}(B \to D^{**}\ell\nu)$	0.5	0.2	0.2	0.2	0.2	0.3	0.3	0.3	0.2	0.3	0.3	0.5	0.2	0.2	0.2	0.2
Nonresonant $b \to c\ell\nu$ BF	0.7	0.3	0.3	0.2	0.3	0.3	0.3	0.3	0.2	0.5	0.1	0.5	0.3	0.2	0.2	0.2
$B \to D\ell\nu$ FF	0.2	0.1	0.2	0.1	0.2	0.1	0.1	0.2	0.3	0.3	0.2	0.5	0.1	0.1	0.2	0.1
$B \to D^*\ell\nu$ FF	0.2	0.1	0.1	0.1	0.1	0.3	0.2	0.4	0.1	0.3	0.5	0.5	0.1	0.1	0.3	0.2
$B \to D^{**}\ell\nu$ FF	0.2	0.0	0.1	0.1	0.7	0.7	0.3	1.2	0.0	0.4	0.6	0.4	0.3	0.4	0.2	0.3
$\Upsilon(4S) \to B^0\bar{B}^0$ BF	1.3	1.6	1.2	1.4	1.4	1.3	1.4	1.3	1.3	1.1	0.9	0.7	1.4	1.4	1.1	1.3
Secondary lepton	2.6	1.8	1.7	1.3	1.4	0.7	0.5	0.6	0.2	1.3	2.3	0.9	0.9	0.8	1.0	0.8
Final state radiation	0.0	1.9	1.1	1.5	1.1	1.2	1.1	1.1	1.5	0.2	1.6	1.4	1.2	1.1	1.2	1.1
B counting	0.6	0.6	0.6	0.6	0.6	0.6	0.6	0.6	0.6	0.6	0.6	0.6	0.6	0.6	0.6	0.6
Fit bias	1.1	0.1	0.3	0.2	0.0	0.3	0.3	0.2	0.9	0.2	0.6	0.0	0.1	0.0	0.4	0.1
Signal MC stat error	1.5	1.6	1.4	1.4	1.4	1.5	1.6	1.5	1.4	1.7	1.2	1.6	0.6	0.4	0.6	0.3
Total systematic error	11.4	5.4	4.5	5.1	5.8	5.0	4.5	5.5	4.9	14.7	7.8	25.4	4.4	4.4	4.6	3.8
Fit error	14.2	11.6	9.9	9.0	9.9	9.1	12.1	12.4	11.6	16.1	13.0	23.9	4.3	3.8	6.7	3.5
Total error	18.2	12.8	10.9	10.3	11.5	10.4	13.0	13.6	12.6	21.8	15.2	34.9	6.2	5.8	8.1	5.1

TABLE XXV: $B^+ \to \pi^0 \ell^+ \nu$ yields, efficiencies (%), $\Delta\mathcal{B}$ (10^{-7}) and their relative uncertainties (%). The $\Delta\mathcal{B}$ and efficiency values labeled "without FSR" are modified to remove FSR effects. This procedure has no significant impact on the $\Delta\mathcal{B}$ values.

q^2 bins (GeV^2)	0-2	2-4	4-6	6-8	8-10	10-12	12-14	14-16	16-18	18-20	20-26.4	q^2<12	q^2<16	q^2>16	Total
Fitted yield	236.3	386.7	452.2	449.2	351.3	320.5	230.8	189.9	156.0	138.8	292.5	2196.1	2616.8	587.3	3204.1
Yield statistical error	14.5	9.7	9.0	9.3	11.5	11.3	13.3	15.0	18.0	24.9	27.2	4.3	4.9	17.0	5.3
Unfolded yield	259.6	408.5	453.5	448.3	322.9	339.0	225.1	210.0	175.7	140.3	221.4	2231.7	2666.7	537.3	3204.1
Efficiency	4.00	5.14	5.88	6.03	5.21	4.19	3.22	2.81	2.92	3.44	4.18	-	-	-	-
Eff. (without FSR)	3.95	5.15	5.92	6.05	5.24	4.19	3.22	2.80	2.93	3.45	4.15	-	-	-	-
$\Delta\mathcal{B}$	68.0	83.3	80.9	78.0	65.0	84.8	73.3	78.3	63.1	42.8	55.6	460.0	611.6	161.5	773.1
$\Delta\mathcal{B}$ (without FSR)	68.9	83.2	80.3	77.8	64.6	84.9	73.3	78.6	62.9	42.7	56.0	459.7	611.6	161.5	773.1
Tracking efficiency	2.6	1.6	0.2	0.5	0.9	0.8	0.7	0.8	1.0	2.0	3.6	0.9	0.7	1.0	0.7
Photon efficiency	5.5	5.2	0.6	3.0	1.6	3.1	3.9	2.7	1.4	8.9	5.5	2.6	2.5	1.3	2.2
K^0_L efficiency	1.7	0.5	0.3	0.6	0.5	0.4	0.7	0.8	1.3	1.3	1.3	0.5	0.4	1.0	0.5
K^0_L production spectrum	1.0	0.8	0.9	0.6	0.6	0.7	0.7	0.8	2.2	1.4	1.4	0.3	0.3	1.5	0.5
K^0_L energy	0.7	0.8	0.5	0.3	0.5	0.5	0.4	0.9	0.5	2.1	1.5	0.3	0.3	0.8	0.4
ℓ identification	1.0	0.2	1.5	1.0	1.0	0.7	1.3	1.0	0.8	0.8	2.9	0.6	0.7	1.5	0.9
Bremsstrahlung	0.1	0.1	0.1	0.2	0.2	0.1	0.3	0.1	0.2	1.1	0.4	0.1	0.1	0.4	0.2
q^2 continuum shape	9.7	2.7	3.3	2.9	1.8	0.6	0.1	1.0	3.7	12.9	12.2	1.2	0.8	6.9	1.1
$\mathcal{B}(B^0 \to \pi^- \ell^+ \nu)$ BF	0.2	0.1	0.1	0.1	0.2	0.1	0.2	0.1	0.2	0.5	2.5	0.1	0.1	1.0	0.3
$\mathcal{B}(B^0 \to \rho^- \ell^+ \nu)$	0.3	0.2	0.1	0.4	0.1	0.1	0.1	0.4	0.2	2.5	1.1	0.1	0.1	0.4	0.2
$\mathcal{B}(B^+ \to \rho^0 \ell^+ \nu)$	0.1	0.1	0.1	0.1	0.1	0.1	0.1	0.1	0.2	0.6	1.1	0.1	0.1	0.6	0.1
$\mathcal{B}(B^+ \to \omega \ell^+ \nu)$	0.2	0.1	0.1	0.1	0.2	0.2	0.3	0.1	0.5	0.5	2.2	0.1	0.1	1.0	0.2
$\mathcal{B}(B^+ \to \eta \ell^+ \nu)$	0.1	0.1	0.1	0.1	0.1	0.1	0.1	0.2	0.2	0.7	0.5	0.1	0.1	0.4	0.2
$\mathcal{B}(B^+ \to \eta' \ell^+ \nu)$	0.1	0.1	0.1	0.1	0.1	0.1	0.1	0.2	0.2	0.4	0.3	0.1	0.1	0.3	0.1
Nonresonant $b \to u \ell \nu$ BF	0.2	0.1	0.2	0.4	0.4	0.4	0.2	0.6	0.2	1.6	3.1	0.2	0.3	1.4	0.5
SF parameters	1.6	0.5	0.7	0.7	0.8	0.3	0.8	1.8	1.2	0.6	14.0	0.6	0.2	4.5	1.0
$B \to \rho \ell \nu$ FF	0.1	1.7	1.9	2.2	3.0	0.8	1.6	0.5	0.7	4.0	6.6	1.6	1.4	1.6	1.4
$B^+ \to \pi^0 \ell^+ \nu$ FF	0.1	0.1	0.1	0.1	0.1	0.1	0.1	0.1	0.2	0.6	0.5	0.1	0.1	0.4	0.2
$B^+ \to \eta^{(\prime)} \ell^+ \nu$ FF	0.1	0.1	0.1	0.1	0.1	0.1	0.1	0.1	0.2	0.6	0.4	0.1	0.1	0.4	0.1
$B^+ \to \omega \ell^+ \nu$ FF	0.4	0.1	0.1	0.1	0.6	0.1	0.2	0.4	0.5	1.4	6.8	0.1	0.1	2.3	0.5
$\mathcal{B}(B \to D \ell \nu)$	0.3	0.2	0.3	0.3	0.5	0.2	0.3	0.1	0.3	0.6	0.3	0.2	0.1	0.3	0.1
$\mathcal{B}(B \to D^* \ell \nu)$	0.2	0.3	0.4	0.4	0.5	0.2	0.2	0.2	0.3	0.5	0.4	0.3	0.2	0.3	0.2
$\mathcal{B}(B \to D^{**} \ell \nu)$	0.4	0.2	0.2	0.2	0.2	0.3	0.3	0.2	0.3	0.7	0.6	0.2	0.2	0.4	0.2
Nonresonant $b \to c \ell \nu$ BF	0.4	0.2	0.2	0.1	0.5	0.2	0.2	0.2	0.3	0.6	0.6	0.2	0.2	0.4	0.2
$B \to D \ell \nu$ FF	0.2	0.1	0.1	0.1	0.2	0.2	0.1	0.1	0.2	0.5	0.9	0.1	0.1	0.5	0.2
$B \to D^* \ell \nu$ FF	0.2	0.1	0.2	0.3	0.5	0.2	0.2	0.2	0.2	0.5	1.3	0.2	0.2	0.5	0.2
$B \to D^{**} \ell \nu$ FF	0.4	0.2	0.2	0.2	0.2	0.3	0.3	0.2	0.3	0.7	0.6	0.3	0.2	0.4	0.2
$\Upsilon(4S) \to B^0 \bar{B}^0$ BF	1.4	1.2	1.3	1.3	1.3	1.3	1.1	1.3	1.1	1.4	1.3	1.3	1.3	1.2	1.3
Secondary lepton	1.6	0.2	0.4	0.3	0.9	0.3	0.4	0.4	0.6	1.3	1.7	0.4	0.3	0.9	0.4
Final state radiation	0.2	1.2	1.9	0.7	2.3	1.2	2.5	1.0	0.4	2.1	0.2	1.3	1.4	0.8	1.3
B counting	0.6	0.6	0.6	0.6	0.6	0.6	0.6	0.6	0.6	0.6	0.6	0.6	0.6	0.6	0.6
Signal MC stat error	1.9	1.8	2.3	1.7	2.6	2.1	2.8	2.6	2.5	2.4	1.5	0.8	0.5	0.9	0.4
Total systematic error	12.1	6.9	5.5	5.7	5.9	4.7	6.2	5.2	6.0	17.9	24.2	4.4	3.8	10.1	4.0
Fit error	17.0	14.1	14.9	15.3	20.0	16.5	20.9	21.2	25.8	40.7	39.4	6.6	5.3	17.8	5.7
Total error	20.9	15.7	15.9	16.4	20.9	17.1	21.9	21.9	26.5	44.5	46.3	7.9	6.5	20.4	6.9

TABLE XXVI: $B^+ \to \omega\ell^+\nu$ and combined $B^+ \to \eta\ell^+\nu$ (3π and $\gamma\gamma$ decay channels) yields, efficiencies(%), $\Delta\mathcal{B}$ (10^{-7}) and their relative uncertainties (%).

Decay mode	$\omega\ell^+\nu$						$\eta\ell^+\nu$ (3π and $\gamma\gamma$ combined)					
q^2 bins (GeV^2)	0-4	4-8	8-12	12-16	16-20.2	0-20.2	0-4	4-8	8-2	12-16	16-22.4	0-22.4
Fitted yield	292.6	567.5	217.6	253.5	529.7	1860.8	231.4	348.1	153.1	93.7	41.0	867.3
Yield statistical error	20.5	12.1	18.5	23.4	27.6	12.5	20.9	13.9	23.8	36.2	69.6	11.6
Unfolded yield	282.2	590.8	267.7	301.7	418.5	1860.8	231.4	349.8	155.7	96.1	34.3	867.3
Efficiency	2.14	2.19	0.99	1.28	1.83	-	2.64	3.48	1.93	1.51	1.20	-
$\Delta\mathcal{B}$	138.1	283.0	284.6	246.7	239.8	1192.2	91.7	105.4	84.7	66.8	30.0	378.6
Tracking efficiency	6.1	2.0	2.2	5.9	2.6	2.3	3.1	0.2	1.2	2.4	17.3	1.1
Photon efficiency	9.6	3.6	8.5	9.7	15.3	1.8	10.8	5.2	3.2	6.4	38.3	5.7
K_L^0 efficiency	0.8	0.9	0.6	1.7	2.6	0.8	1.8	0.4	1.4	3.6	5.3	0.9
K_L^0 production spectrum	1.8	1.1	1.2	1.5	2.3	0.8	1.5	1.5	1.7	1.8	12.4	1.4
K_L^0 energy	1.0	0.6	1.0	1.4	2.2	0.8	1.1	0.5	0.4	2.9	10.1	1.1
ℓ identification	1.9	0.2	1.6	2.4	2.5	0.7	0.3	1.5	1.8	3.7	23.6	3.3
π identification	0.4	0.3	0.3	0.4	0.5	0.4	0.3	0.1	0.2	0.5	3.9	0.5
Bremsstrahlung	0.3	0.1	0.2	0.3	0.6	0.2	0.6	0.2	0.3	0.7	0.8	0.3
q^2 continuum shape	4.6	2.4	4.5	11.0	21.1	3.2	-	-	-	-	-	-
$\mathcal{B}(B^0 \to \pi^-\ell^+\nu)$	0.2	0.1	0.1	0.4	0.6	0.2	0.1	0.0	0.0	0.1	3.5	0.2
$\mathcal{B}(B^+ \to \pi^0\ell^+\nu)$	0.2	0.0	0.1	0.2	0.6	0.2	0.4	0.7	1.3	3.0	13.5	2.2
$\mathcal{B}(B^0 \to \rho^-\ell^+\nu)$	1.1	0.3	0.2	0.9	6.4	1.4	0.4	0.2	0.6	2.2	36.2	3.4
$\mathcal{B}(B^+ \to \rho^0\ell^+\nu)$	0.3	0.1	0.2	0.3	1.8	0.3	0.1	0.1	0.1	0.3	8.9	0.7
$\mathcal{B}(B^+ \to \omega\ell^+\nu)$	-	-	-	-	-	-	0.2	0.4	0.2	1.3	21.1	2.1
$\mathcal{B}(B^+ \to \eta\ell^+\nu)$	0.2	0.1	0.1	0.2	0.8	0.2	-	-	-	-	-	-
$\mathcal{B}(B^+ \to \eta'\ell^+\nu)$	0.3	0.0	0.1	0.3	0.4	0.2	0.2	0.1	0.1	0.3	3.1	0.4
Nonresonant $b \to u\ell\nu$ BF	1.1	0.3	0.2	0.5	5.7	1.0	0.6	0.6	1.4	3.8	46.8	5.0
η and ω BFs	1.1	0.6	1.0	0.6	0.4	0.7	0.5	0.6	0.7	0.8	4.8	0.8
SF parameters	0.6	1.0	0.3	4.2	11.5	3.4	1.4	2.0	2.3	3.9	79.2	8.3
$B \to \rho\ell\nu$ FF	2.0	0.2	0.1	1.7	7.8	1.6	0.2	0.9	1.0	0.4	6.8	0.2
$B^0 \to \pi^-\ell^+\nu$ FF	0.1	0.2	0.1	0.4	0.9	0.3	0.3	0.5	0.3	0.3	1.5	0.1
$B^+ \to \eta\ell^+\nu$ FF	0.2	0.1	0.1	0.2	0.6	0.2	1.9	1.7	1.5	1.0	0.8	1.4
$B^+ \to \omega\ell^+\nu$ FF	22.6	4.9	9.1	11.3	10.0	3.3	0.3	1.4	0.3	0.4	7.1	0.3
$\mathcal{B}(B \to D\ell\nu)$	0.5	0.5	0.3	0.3	0.8	0.3	0.4	0.7	0.6	0.6	5.8	0.6
$\mathcal{B}(B \to D^*\ell\nu)$	0.6	0.2	0.3	0.7	1.3	0.5	0.4	0.6	0.4	1.2	5.2	0.6
$\mathcal{B}(B \to D^{**}\ell\nu)$	0.7	0.4	0.5	0.4	1.5	0.3	0.7	0.3	0.3	0.6	4.4	0.5
Nonresonant $b \to c\ell\nu$ BF	0.6	0.2	0.2	0.3	1.2	0.2	0.9	0.2	0.6	0.6	3.4	0.3
$B \to D\ell\nu$ FF	0.8	0.5	0.2	0.3	0.4	0.2	0.2	0.1	0.8	0.6	4.1	0.4
$B \to D^*\ell\nu$ FF	0.5	0.5	0.3	0.8	2.7	0.8	0.5	0.5	0.8	1.3	9.5	0.7
$B \to D^{**}\ell\nu$ FF	1.3	1.1	0.2	0.3	1.2	0.3	0.3	2.3	0.2	1.6	0.7	0.7
$\mathcal{B}(\Upsilon(4S) \to B^0\bar{B}^0)$	1.7	1.1	1.1	1.4	0.6	1.1	1.3	1.2	1.6	1.7	4.3	1.5
Secondary lepton	0.9	0.6	0.4	1.8	2.6	0.6	1.1	0.5	0.8	5.7	11.1	1.8
Final state radiation	1.3	2.6	1.8	2.5	3.1	1.0	4.2	3.1	2.0	3.7	17.4	0.3
B counting	0.6	0.6	0.6	0.6	0.6	0.6	0.6	0.6	0.6	0.6	0.6	0.6
Signal MC stat error	2.0	1.7	3.2	3.0	2.3	0.8	1.7	1.4	1.8	1.4	0.4	0.6
Total systematic error	26.3	8.1	14.2	20.9	33.5	7.4	12.8	7.6	7.2	13.8	117.5	13.2
Fit error	24.6	14.0	23.7	31.8	35.9	13.0	23.5	15.9	28.4	42.3	92.5	13.7
Total error	36.0	16.1	27.6	38.1	49.1	15.0	26.8	17.6	29.3	44.5	149.5	19.0

TABLE XXVII: $B^+ \to \eta^{(\prime)}\ell^+\nu$ yields, efficiencies(%), $\Delta\mathcal{B}$ (10^{-7}) and their relative uncertainties (%).

Decay mode	$\eta'\ell^+\nu$	$\eta\ell^+\nu$ (3π)	$\eta\ell^+\nu$ ($\gamma\gamma$)					
q^2 bins (GeV^2)	0-18.7	0-22.4	0-4	4-8	8-12	12-16	16-22.4	0-22.4
Fitted yield	141.1	279.8	192.3	186.1	105.5	49.5	36.8	570.1
Yield statistical error	25.6	22.1	22.4	21.6	27.9	50.4	71.2	15.3
Unfolded yield	141.1	279.8	201.7	173.5	112.6	46.8	35.5	570.1
Efficiency	0.61	0.63	1.99	2.56	1.32	1.03	0.89	-
$\Delta\mathcal{B}$	242.3	464.4	106.4	71.2	89.7	47.5	42.0	356.9
Tracking efficiency	4.1	1.0	2.1	0.7	3.0	5.5	9.3	0.8
Photon efficiency	3.3	3.9	8.5	8.3	7.7	22.1	28.1	8.5
K_L^0 efficiency	1.2	1.2	1.8	1.1	1.0	3.8	3.2	1.0
K_L^0 production spectrum	2.8	0.7	1.5	3.1	1.8	4.2	12.3	1.9
K_L^0 energy	1.2	0.7	1.5	1.1	0.7	7.1	6.5	1.3
ℓ identification	2.5	3.7	0.3	1.9	2.0	1.8	18.0	3.2
π identification	0.7	0.6	-	-	-	-	-	-
Bremsstrahlung	0.5	0.3	0.3	0.3	0.2	1.0	0.3	0.2
Continuum yield	5.8	3.3	-	-	-	-	-	-
$\mathcal{B}(B^0 \to \pi^-\ell^+\nu)$	0.0	0.1	0.2	0.1	0.1	0.3	2.7	0.4
$\mathcal{B}(B^+ \to \pi^0\ell^+\nu)$	0.2	0.1	0.5	1.4	1.7	5.9	12.4	3.1
$\mathcal{B}(B^+ \to \eta^{(\prime)}\ell^+\nu)$	0.4	0.4	0.2	0.3	0.1	0.6	2.1	0.4
$\mathcal{B}(B^0 \to \rho^-\ell^+\nu)$	0.7	1.5	0.5	0.4	0.8	3.6	23.4	3.4
$\mathcal{B}(B^+ \to \rho^0\ell^+\nu)$	0.0	0.6	0.1	0.1	0.2	0.7	5.2	0.6
$\mathcal{B}(B^+ \to \omega\ell^+\nu)$	1.4	1.6	0.2	0.7	0.2	1.1	10.3	1.6
Nonresonant $b \to u\ell\nu$ BF	3.2	3.5	0.2	1.0	1.5	4.7	29.7	4.7
η BF	2.0	1.3	0.6	0.7	0.7	0.7	1.7	0.6
SF parameters	4.3	7.4	0.8	2.7	1.9	3.4	49.3	7.4
$B \to \rho\ell\nu$ FF	0.1	1.4	0.2	1.5	0.8	0.7	4.5	0.2
$B^0 \to \pi^-\ell^+\nu$ FF	0.0	0.0	0.0	0.1	0.0	0.2	0.9	0.1
$B^+ \to \eta\ell^+\nu$ FF	0.9	0.9	0.1	0.1	0.1	0.7	1.8	0.4
$B^+ \to \omega\ell^+\nu$ FF	0.9	2.2	0.5	2.3	0.7	1.0	3.6	0.3
$\mathcal{B}(B \to D\ell\nu)$	0.6	0.8	0.4	0.7	0.2	1.4	4.5	0.6
$\mathcal{B}(B \to D^*\ell\nu)$	0.3	0.4	0.2	0.8	0.1	2.2	3.9	0.6
$\mathcal{B}(B \to D^{**}\ell\nu)$	0.6	0.2	0.5	0.3	0.5	1.2	2.5	0.5
Nonresonant $b \to c\ell\nu$ BF	0.1	0.1	0.4	0.5	0.3	1.2	2.8	0.6
$B \to D\ell\nu$ FF	0.1	0.1	0.2	0.2	0.5	0.7	2.7	0.4
$B \to D^*\ell\nu$ FF	0.4	0.5	0.3	0.5	0.2	2.6	7.7	1.1
$B \to D^{**}\ell\nu$ FF	0.5	0.1	0.5	1.0	1.0	1.4	3.1	0.1
$\mathcal{B}(\Upsilon(4S) \to B^0\bar{B}^0)$	1.3	1.0	1.4	1.4	1.7	3.4	3.2	1.9
Secondary lepton	3.2	1.7	1.3	0.9	0.5	7.6	3.5	1.1
Final state radiation	1.5	1.0	4.2	3.0	2.3	3.8	17.1	0.1
B counting	0.6	0.6	0.6	0.6	0.6	0.6	0.6	0.6
Signal MC stat error	1.4	1.0	1.9	1.8	2.1	1.8	0.4	0.7
Total systematic error	11.5	11.2	10.6	11.0	10.2	28.2	77.7	14.1
Fit error	34.9	22.1	24.0	26.4	31.4	62.4	81.8	17.7
Total error	36.7	24.8	26.2	28.6	33.0	68.5	112.9	22.7

TABLE XXVIII: Correlation matrix of the partial $\Delta\mathcal{B}(B \to \pi\ell^+\nu, q^2)$ statistical uncertainties.

q^2 bins (GeV^2)	0-2	2-4	4-6	6-8	8-10	10-12	12-14	14-16	16-18	18-20	20-22	22-26.4
0-2	1.00	-0.11	0.20	0.02	-0.01	0.03	0.01	0.03	0.05	0.09	0.08	-0.02
2-4	-0.11	1.00	-0.31	0.14	-0.02	0.01	-0.00	0.01	0.02	0.03	0.03	-0.01
4-6	0.20	-0.31	1.00	-0.30	0.16	0.02	0.06	0.05	0.07	0.02	0.02	-0.00
6-8	0.02	0.14	-0.30	1.00	-0.24	0.14	0.06	0.05	0.07	0.00	0.01	0.00
8-10	-0.01	-0.02	0.16	-0.24	1.00	-0.24	0.16	0.04	0.07	-0.01	-0.01	0.01
10-12	0.03	0.01	0.02	0.14	-0.24	1.00	-0.18	0.09	0.07	0.00	0.02	-0.00
12-14	0.01	-0.00	0.06	0.06	0.16	-0.18	1.00	-0.20	0.13	-0.01	0.03	-0.01
14-16	0.03	0.01	0.05	0.05	0.04	0.09	-0.20	1.00	-0.06	0.01	-0.02	-0.01
16-18	0.05	0.02	0.07	0.07	0.07	0.07	0.13	-0.06	1.00	-0.19	0.09	-0.06
18-20	0.09	0.03	0.02	0.00	-0.01	0.00	-0.01	0.01	-0.19	1.00	0.03	-0.06
20-22	0.08	0.03	0.02	0.01	-0.01	0.02	0.03	-0.02	0.09	0.03	1.00	-0.37
22-26.4	-0.02	-0.01	-0.00	0.00	0.01	-0.00	-0.01	-0.01	-0.06	-0.06	-0.37	1.00

TABLE XXIX: Correlation matrix of the partial $\Delta\mathcal{B}(B^0 \to \pi^-\ell^+\nu, q^2)$ statistical uncertainties.

q^2 bins (GeV^2)	0-2	2-4	4-6	6-8	8-10	10-12	12-14	14-16	16-18	18-20	20-22	22-26.4
0-2	1.00	-0.07	0.20	0.02	-0.01	0.03	0.01	0.03	0.05	0.07	0.06	-0.01
2-4	-0.07	1.00	-0.28	0.12	-0.02	0.00	-0.01	0.01	0.02	0.02	0.02	-0.01
4-6	0.20	-0.28	1.00	-0.29	0.14	0.02	0.05	0.05	0.07	0.02	0.02	0.00
6-8	0.02	0.12	-0.29	1.00	-0.22	0.13	0.06	0.05	0.06	0.00	0.01	0.00
8-10	-0.01	-0.02	0.14	-0.22	1.00	-0.23	0.15	0.04	0.06	-0.01	-0.00	0.01
10-12	0.03	0.00	0.02	0.13	-0.23	1.00	-0.16	0.08	0.07	0.00	0.02	-0.00
12-14	0.01	-0.01	0.05	0.06	0.15	-0.16	1.00	-0.18	0.13	-0.00	0.04	-0.01
14-16	0.03	0.01	0.05	0.05	0.04	0.08	-0.18	1.00	-0.04	0.01	-0.01	-0.01
16-18	0.05	0.02	0.07	0.06	0.06	0.07	0.13	-0.04	1.00	-0.16	0.10	-0.05
18-20	0.07	0.02	0.02	0.00	-0.01	0.00	-0.00	0.01	-0.16	1.00	0.05	-0.05
20-22	0.06	0.02	0.02	0.01	-0.00	0.02	0.04	-0.01	0.10	0.05	1.00	-0.30
22-26.4	-0.01	-0.01	0.00	0.00	0.01	-0.00	-0.01	-0.01	-0.05	-0.05	-0.30	1.00

TABLE XXX: Correlation matrix of the partial $\Delta\mathcal{B}(B^+ \to \pi^0\ell^+\nu, q^2)$ statistical uncertainties.

q^2 bins (GeV^2)	0-2	2-4	4-6	6-8	8-10	10-12	12-14	14-16	16-18	18-20	20-26.4
0-2	1.00	-0.21	0.17	0.01	0.03	0.01	0.01	0.01	0.04	0.05	0.02
2-4	-0.21	1.00	-0.37	0.18	-0.02	0.02	0.01	0.02	0.03	0.03	0.01
4-6	0.17	-0.37	1.00	-0.40	0.18	-0.01	0.04	0.03	0.04	0.04	-0.01
6-8	0.01	0.18	-0.40	1.00	-0.38	0.16	-0.00	0.04	0.03	0.03	-0.02
8-10	0.03	-0.02	0.18	-0.38	1.00	-0.33	0.15	0.02	0.04	0.04	-0.05
10-12	0.01	0.02	-0.01	0.16	-0.33	1.00	-0.32	0.12	0.01	0.03	-0.04
12-14	0.01	0.01	0.04	-0.00	0.15	-0.32	1.00	-0.28	0.09	0.02	-0.03
14-16	0.01	0.02	0.03	0.04	0.02	0.12	-0.28	1.00	-0.23	0.07	-0.03
16-18	0.04	0.03	0.04	0.03	0.04	0.01	0.09	-0.23	1.00	-0.20	0.03
18-20	0.05	0.03	0.04	0.03	0.04	0.03	0.02	0.07	-0.20	1.00	-0.18
20-26.4	0.02	0.01	-0.01	-0.02	-0.05	-0.04	-0.03	-0.03	0.03	-0.18	1.00

TABLE XXXI: Correlation matrix of the partial $\Delta\mathcal{B}(B \to \pi\ell^+\nu, q^2)$ systematic uncertainties.

q^2 bins (GeV^2)	0-2	2-4	4-6	6-8	8-10	10-12	12-14	14-16	16-18	18-20	20-22	22-26.4
0-2	1.00	0.02	0.10	0.39	0.51	0.35	0.58	0.43	0.09	0.10	0.29	-0.15
2-4	0.02	1.00	0.55	0.67	0.37	0.46	0.49	0.43	0.08	0.03	0.35	-0.06
4-6	0.10	0.55	1.00	0.61	0.60	0.32	0.49	0.53	-0.05	0.30	0.52	-0.21
6-8	0.39	0.67	0.61	1.00	0.41	0.78	0.52	0.41	0.34	-0.05	0.47	0.08
8-10	0.51	0.37	0.60	0.41	1.00	-0.00	0.78	0.88	-0.36	0.58	0.58	-0.49
10-12	0.35	0.46	0.32	0.78	-0.00	1.00	0.28	0.08	0.65	-0.32	0.22	0.27
12-14	0.58	0.49	0.49	0.52	0.78	0.28	1.00	0.80	-0.03	0.44	0.41	-0.41
14-16	0.43	0.43	0.53	0.41	0.88	0.08	0.80	1.00	-0.30	0.63	0.53	-0.61
16-18	0.09	0.08	-0.05	0.34	-0.36	0.65	-0.03	-0.30	1.00	-0.53	-0.01	0.57
18-20	0.10	0.03	0.30	-0.05	0.58	-0.32	0.44	0.63	-0.53	1.00	0.35	-0.67
20-22	0.29	0.35	0.52	0.47	0.58	0.22	0.41	0.53	-0.01	0.35	1.00	-0.15
22-26.4	-0.15	-0.06	-0.21	0.08	-0.49	0.27	-0.41	-0.61	0.57	-0.67	-0.15	1.00

TABLE XXXII: Correlation matrix of the partial $\Delta\mathcal{B}(B^0 \to \pi^-\ell^+\nu, q^2)$ systematic uncertainties.

q^2 bins (GeV^2)	0-2	2-4	4-6	6-8	8-10	10-12	12-14	14-16	16-18	18-20	20-22	22-26.4
0-2	1.00	-0.10	0.10	0.42	0.60	0.42	0.57	0.47	0.18	0.11	0.31	-0.19
2-4	-0.10	1.00	0.48	0.59	0.41	0.48	0.47	0.45	0.18	0.05	0.30	-0.05
4-6	0.10	0.48	1.00	0.69	0.55	0.46	0.35	0.41	0.10	0.16	0.44	0.10
6-8	0.42	0.59	0.69	1.00	0.75	0.75	0.66	0.65	0.27	0.08	0.61	-0.06
8-10	0.60	0.41	0.55	0.75	1.00	0.54	0.74	0.85	0.09	0.33	0.49	-0.35
10-12	0.42	0.48	0.46	0.75	0.54	1.00	0.57	0.49	0.49	-0.17	0.59	0.07
12-14	0.57	0.47	0.35	0.66	0.74	0.57	1.00	0.72	0.33	0.21	0.36	-0.29
14-16	0.47	0.45	0.41	0.65	0.85	0.49	0.72	1.00	0.15	0.40	0.40	-0.46
16-18	0.18	0.18	0.10	0.27	0.09	0.49	0.33	0.15	1.00	-0.37	0.47	0.25
18-20	0.11	0.05	0.16	0.08	0.33	-0.17	0.21	0.40	-0.37	1.00	-0.38	-0.71
20-22	0.31	0.30	0.44	0.61	0.49	0.59	0.36	0.40	0.47	-0.38	1.00	0.33
22-26.4	-0.19	-0.05	0.10	-0.06	-0.35	0.07	-0.29	-0.46	0.25	-0.71	0.33	1.00

TABLE XXXIII: Correlation matrix of the partial $\Delta\mathcal{B}(B^+ \to \pi^0\ell^+\nu, q^2)$ systematic uncertainties.

q^2 bins (GeV^2)	0-2	2-4	4-6	6-8	8-10	10-12	12-14	14-16	16-18	18-20	20-26.4
0-2	1.00	0.25	-0.32	-0.06	-0.25	0.27	0.28	0.04	0.07	0.15	-0.31
2-4	0.25	1.00	0.40	0.76	0.21	0.65	0.60	0.12	0.01	0.16	0.01
4-6	-0.32	0.40	1.00	0.59	0.63	0.34	0.31	0.18	0.02	-0.17	0.34
6-8	-0.06	0.76	0.59	1.00	0.40	0.63	0.53	0.17	0.17	0.18	0.25
8-10	-0.25	0.21	0.63	0.40	1.00	0.19	0.25	0.13	0.00	-0.15	0.42
10-12	0.27	0.65	0.34	0.63	0.19	1.00	0.61	0.39	0.32	0.38	0.01
12-14	0.28	0.60	0.31	0.53	0.25	0.61	1.00	0.28	0.22	0.36	-0.08
14-16	0.04	0.12	0.18	0.17	0.13	0.39	0.28	1.00	0.31	0.32	-0.18
16-18	0.07	0.01	0.02	0.17	0.00	0.32	0.22	0.31	1.00	0.59	-0.06
18-20	0.15	0.16	-0.17	0.18	-0.15	0.38	0.36	0.32	0.59	1.00	-0.08
20-26.4	-0.31	0.01	0.34	0.25	0.42	0.01	-0.08	-0.18	-0.06	-0.08	1.00

TABLE XXXIV: Correlation matrix of the partial $\Delta\mathcal{B}(B^+ \to \omega\ell^+\nu, q^2)$ statistical and systematic uncertainties.

	Statistical					Systematic				
q^2 bins (GeV^2)	0-4	4-8	8-12	12-16	16-20.2	0-4	4-8	8-12	12-16	16-20.2
0-4	1.00	-0.12	0.07	0.10	-0.02	1.00	0.23	-0.25	-0.20	-0.38
4-8	-0.12	1.00	-0.13	0.03	0.08	0.23	1.00	-0.53	-0.62	0.17
8-12	0.07	-0.13	1.00	-0.08	0.19	-0.25	-0.53	1.00	0.82	-0.16
12-16	0.10	0.03	-0.08	1.00	0.12	-0.20	-0.62	0.82	1.00	-0.22
16-20.2	-0.02	0.08	0.19	0.12	1.00	-0.38	0.17	-0.16	-0.22	1.00

TABLE XXXV: Correlation matrix of the partial $\Delta\mathcal{B}(B^+ \to \eta\ell^+\nu, q^2)$ statistical and systematic uncertainties.

	Statistical					Systematic				
q^2 bins (GeV^2)	0-4	4-8	8-12	12-16	16-22.4	0-4	4-8	8-12	12-16	16-22.4
0-4	1.00	-0.04	0.02	-0.02	0.06	1.00	-0.31	0.46	0.23	0.26
4-8	-0.04	1.00	-0.12	0.06	0.06	-0.31	1.00	0.12	-0.17	0.00
8-12	0.02	-0.12	1.00	-0.07	0.06	0.46	0.12	1.00	0.45	0.49
12-16	-0.02	0.06	-0.07	1.00	-0.14	0.23	-0.17	0.45	1.00	0.62
16-22.4	0.06	0.06	0.06	-0.14	1.00	0.26	0.00	0.49	0.62	1.00

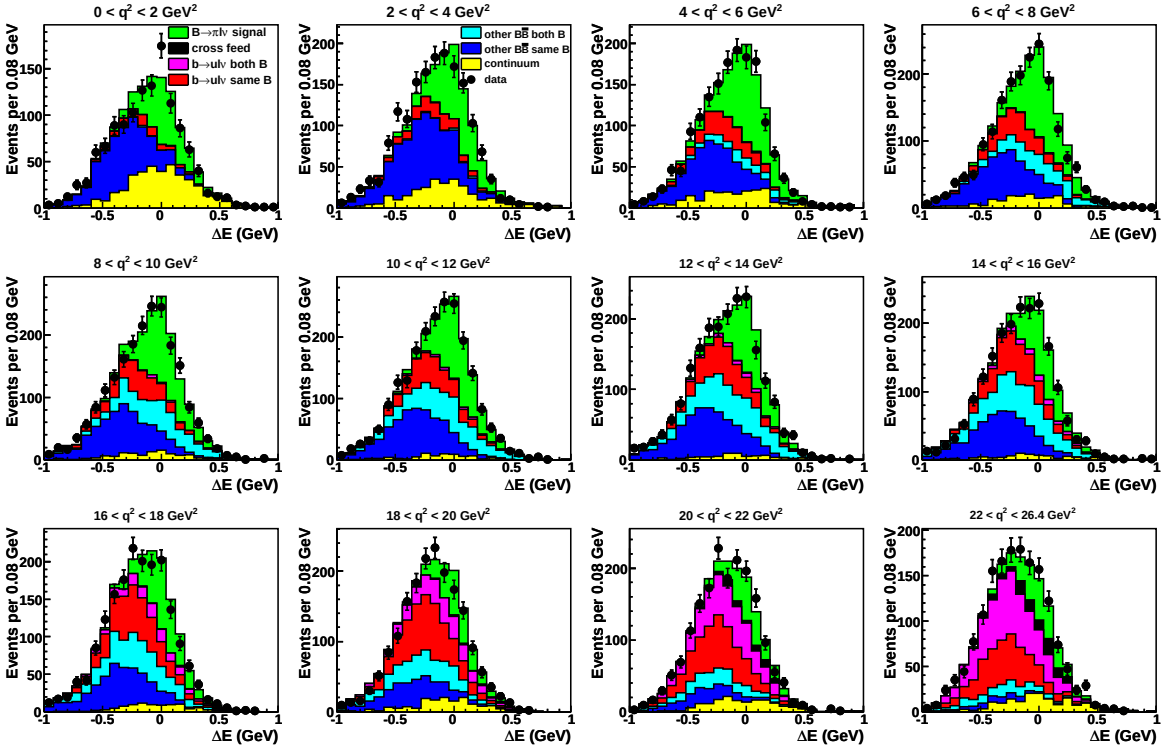

FIG. 13: (color online) ΔE yield fit projections in the signal-enhanced region, with $m_{ES} > 5.2675$ GeV, obtained in 12 q^2 bins from the fit to the experimental data for combined $B^0 \to \pi^-\ell^+\nu$ and $B^+ \to \pi^0\ell^+\nu$ decays. The fit was done using the full ΔE-m_{ES} fit region.

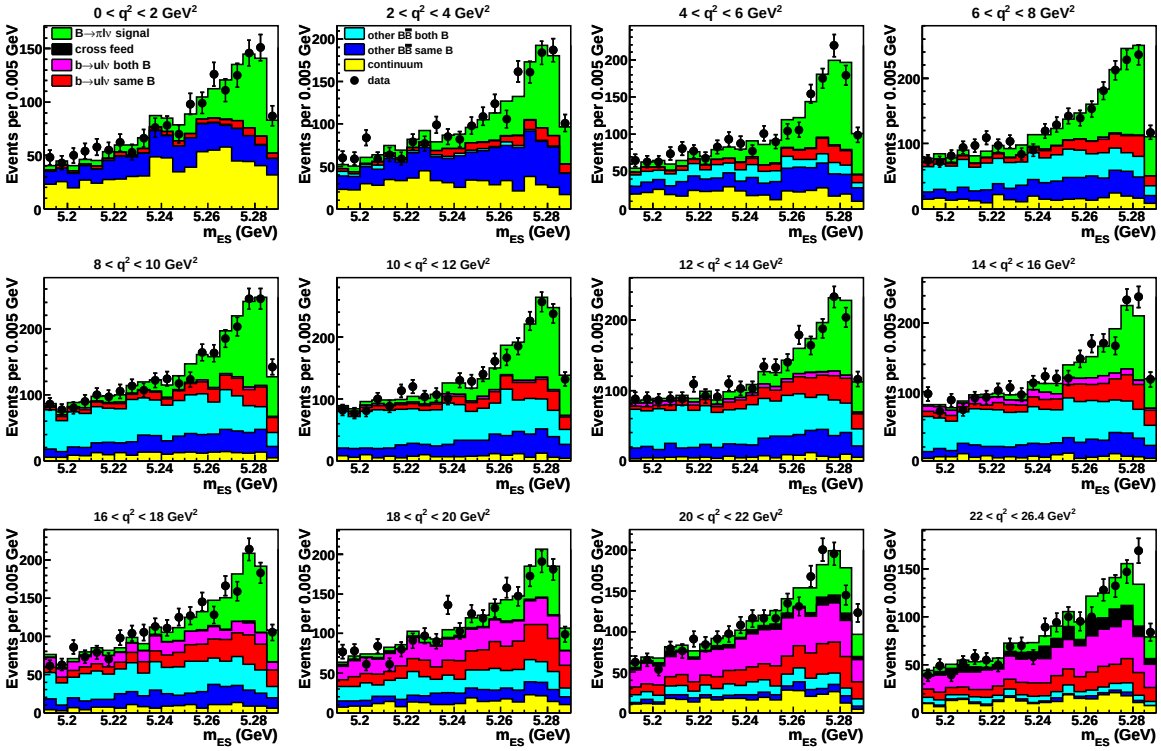

FIG. 14: (color online) m_{ES} yield fit projections in the signal-enhanced region, with $-0.16 < \Delta E < 0.20$ GeV, obtained in 12 q^2 bins from the fit to the experimental data for combined $B^0 \to \pi^- \ell^+ \nu$ and $B^+ \to \pi^0 \ell^+ \nu$ decays. The fit was done using the full ΔE-m_{ES} fit region.

[1] N. Cabibbo, Phys. Lett. **10**, 531 (1963); M. Kobayashi and T. Maskawa, Prog. Theor. Phys. **49**, 652 (1973).
[2] G. Duplancic, A. Khodjamirian, T. Mannel, B. Melic and N. Offen, JHEP **04**, 014 (2008).
[3] A. Khodjamirian, T. Mannel, N. Offen and Y. M. Wang, Phys. Rev. **D83**, 094031 (2011).
[4] P. Ball and G. W. Jones, JHEP **08**, 025 (2007).
[5] E. Gulez *et al.* (HPQCD Collaboration), Phys. Rev. **D73**, 074502 (2006); Erratum ibid. **D75**, 119906 (2007).
[6] J. A. Bailey *et al.* (FNAL/MILC Collaboration), Phys. Rev. **D79**, 054507 (2009); C. Bernard *et al.* (FNAL/MILC Collaboration), Phys. Rev. **D80**, 034026 (2009); R. Van de Water, private communication.
[7] Charge conjugate decays are implied throughout this paper.
[8] P. del Amo Sanchez *et al.* (*BABAR* Collaboration), Phys. Rev. **D83**, 032007 (2011).
[9] P. del Amo Sanchez *et al.* (*BABAR* Collaboration), Phys. Rev. **D83**, 052011 (2011).
[10] H. Ha *et al.* (Belle Collaboration), Phys. Rev. **D83**, 071101 (2011).
[11] J. P. Lees *et al.* (*BABAR* Collaboration), arXiv:1205.6245v1; Phys. Rev. **D** to be published.
[12] K. Nakamura *et al.* (Particle Data Group), Jour. of Phys. **G37**, 075021 (2010); see, in particular, the section "Determination of $|V_{cb}|$ and $|V_{ub}|$."
[13] C. di Donato, G. Ricciardi and I. I. Bigi, Phys. Rev. **D85**, 013016 (2012).
[14] B. Aubert *et al.* (*BABAR* Collaboration), Phys. Rev. Lett. **98**, 091801 (2007).
[15] B. Aubert *et al.* (*BABAR* Collaboration), Nucl. Instrum. Methods **A479**, 1 (2002).
[16] D. Côté, S. Brunet, P. Taras and B. Viaud, Eur. Phys. J. C **38**, 105 (2004).
[17] C. G. Boyd and M. J. Savage, Phys. Rev. **D56**, 303 (1997).
[18] P. Ball and R. Zwicky, Phys. Rev. **D71**, 014029 (2005).
[19] D. Becirevic and A. B. Kaidalov, Phys. Lett. **B478**, 417 (2000).
[20] S. Agostinelli *et al.*, (GEANT4 Collaboration), Nucl. Instrum. Methods **A506**, 250 (2003).
[21] B. Aubert *et al.* (*BABAR* Collaboration), Phys. Rev. **D74**, 092004 (2006).
[22] G. Cowan, Statistical Data Analysis, Chap. 11, Oxford University Press (1998).
[23] G. C. Fox and S. Wolfram, Phys. Rev. Lett. **41**, 1581 (1978).
[24] B. Aubert *et al.* (*BABAR* Collaboration), Phys. Rev. **D67**, 031101 (2003).
[25] W. D. Hulsbergen, Nucl. Instrum. Methods **A552**, 566 (2005).
[26] A. DeRujula *et al.*, Nucl. Phys. **B138**, 387 (1978).
[27] R.J. Barlow and C. Beeston, Comput. Phys. Commun. **77**, 219 (1993).
[28] O.L. Buchmüller, H.U. Flächer, Phys. Rev. **D73**, 073008 (2006).
[29] E. Barberio and Z. Was, Comput. Phys. Commun. **79**, 291 (1994).
[30] E. Richter-Was *et al.*, Phys. Lett. **B303**, 163 (1993).
[31] I. Narsky, Nucl. Instrum. Methods **A450**, 444 (2000).
[32] N. Isgur and B. M. Wise, Phys. Lett. **B232**, 113 (1989); **B237**, 527 (1990).
[33] T. Becher and R. J. Hill, Phys. Lett. **B633**, 61 (2006).
[34] A. Bharucha, arXiv:1203.1359.